Supplement of Atmos. Chem. Phys. Discuss., 15, 3455–3491, 2015
http://www.atmos-chem-phys-discuss.net/15/3455/2015/
doi:10.5194/acpd-15-3455-2015-supplement

Atmospheric Chemistry and Physics Discussions

Supplement of

Sources and chemical characterization of organic aerosol during the summer in the eastern Mediterranean

E. Kostenidou et al.

Correspondence to: S. N. Pandis (spyros@chemeng.upatras.gr)

Table S1. Correlations of the M-OOA and b-OOA factors (Patras) and the V-OOA factor (Athens) with various VOCs as measured by PTR-MS.

R^2	Patras M-OOA	Patras b-OOA	Athens V-OOA
m/z 43	0.29	0.13	0.39
m/z 47 (formic acid)	0.21	0.09	0.47
m/z 59 (acetone, glyoxal)	0.21	0.35	0.32
m/z 69 (isoprene)	0.21	0.13	0.20
m/z 71 (MVK, MACR)	0.31	0.21	0.20
m/z 73 (MEK)	0.24	0.25	0.29
m/z 75 (hydroxyacetone)	0.29	0.41	0.30
m/z 77 (PAN)	0.16	0.37	0.16
m/z 81 (terpenes)	0.19	0.26	0.12
m/z 87 (MBO, C5, methacrylic acid)	0.29	0.31	0.38
m/z 95 (2 vinyl furan, phenol)	0.17	0.31	0.36
m/z 99 (hexenal)	0.19	0.30	0.42
m/z 101 (isoprene hyperoxides, hexanal)	0.17	0.28	0.35
m/z 103 (MPAN)	0.23	0.28	
m/z 113 (chlorobenzene, terpenes $+O_3$)	0.30	0.37	0.40
m/z 115 (heptanal)	0.16	0.32	0.42
m/z 137 (monoterpenes)	0.20	0.24	0.1
m/z 139 (nopinone)	0.28	0.39	0.19
m/z 151 (pinonaldehyde)	0.17	0.30	0.17

1. CE estimation

For the CE estimation we applied the algorithm of Kostenidou et al. (2007) that combines AMS and SMPS distributions. The organic density is also calculated from the same algorithm. We modified the above code inserting the shape factor (χ) and we executed it for various shape factors. Then we selected the minimum of the errors scores which corresponds to the optimum triplet of CE, organic density and shape factor.

A. Patras

Figure S1 shows the CE and the organic density for χ=1-1.2. The organic density is quite sensitive to different shape factors, while CE changes significantly only for χ>1.1. Selecting the solution that corresponds to the minimum error score and after removing the spikes (for error score>0.2) the organic density becomes noisy with high values (above 2 g cm^{-3}) (Figure S2a). Thus, for the CE and organic density determination we used a shape factor equals to 1 for the Patras data set (Figure S2b and S2c). In this case the organic density is more smoothed and has more meaningful values. Figure S3 illustrates the correlation between the PM_1 AMS sulphate (after CE corrections) and the $PM_{2.5}$ filter sulphate measurements.

B. Athens

For the Athens data we tested various shape factors in the range 1-1.6. Figure S4 depicts the CE and the organic density for χ=1-1.6. As in Patras the organic density is sensitive to the shape factor, while CE changes dramatically for χ>1.3. Choosing the solution that corresponds to the minimum error score (and after scavenging the spikes for error score>0.2) we obtain the optimum organic density (Figure S5a), with an average value 1.15±0.36 g cm^{-3}. If a shape factor of 1 is used the average organic density becomes 0.66 g cm^{-3}, which is quite low. The optimum CE and χ are illustrated in Figures S5b and S5c. If a χ=1 was used then the average CE would be 0.59. Figure S6 shows the correlation between the $PM_{2.5}$ filter sulphate and the CE corrected PM_1 AMS sulphate measurements.

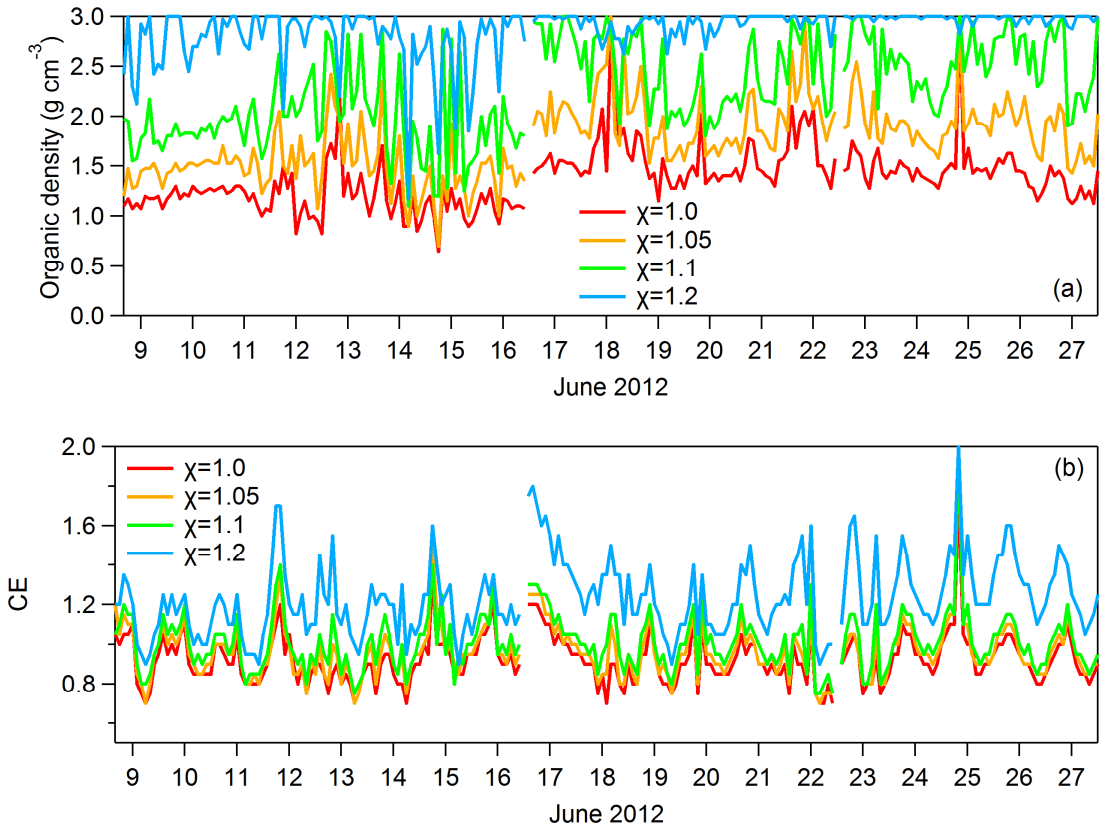

Figure S1. The organic density (a) is sensitive to the shape factor, while CE (b) practically changes for χ greater than 1.1 (Patras).

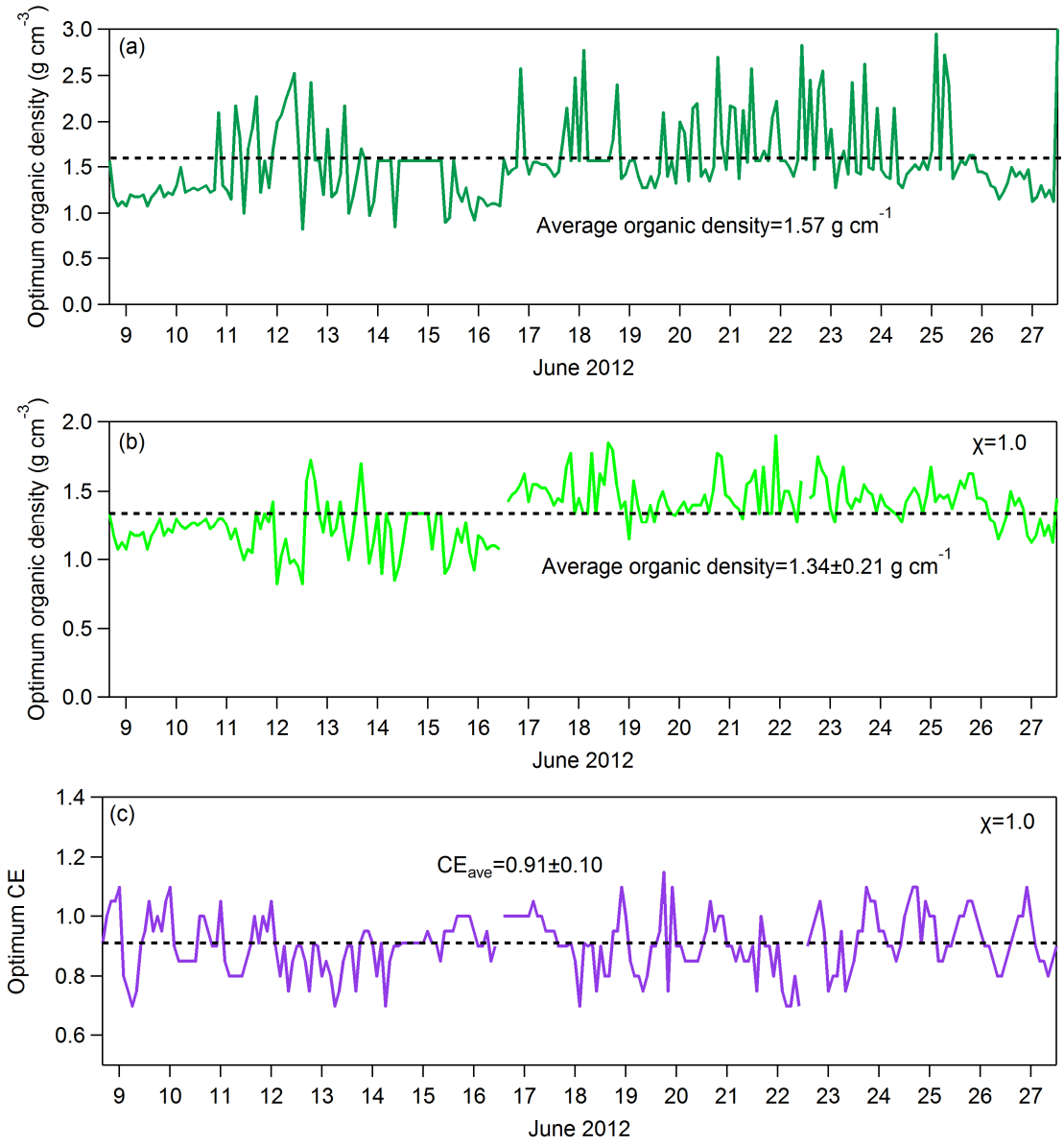

Figure S2. Selecting the solution that corresponds to the minimum error score and after removing the spikes (for error score>0.2) the organic density becomes noisy with values higher than 2 g cm^{-3} (a). Thus we calculated he organic density for χ=1 (b) and the CE for χ=1 (c) (Patras).

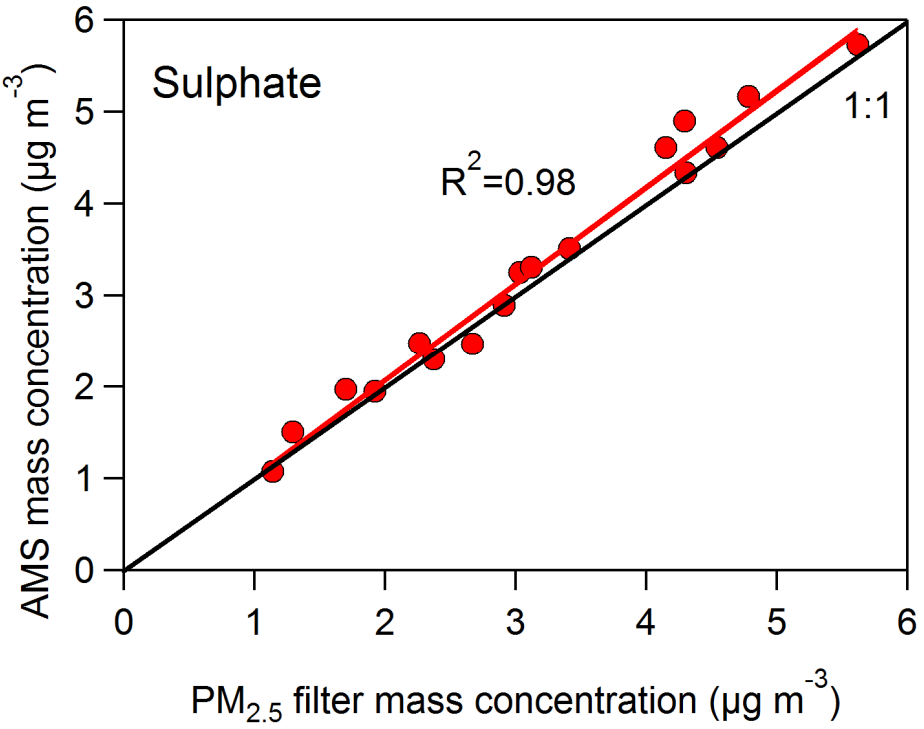

Figure S3. Comparison of the sulphate mass concentration between the PM_1 AMS (after the CE correction) and the $PM_{2.5}$ filters measurements (Patras). The R^2 is 0.98, which suggest that there was almost no sulphate in the coarse mode.

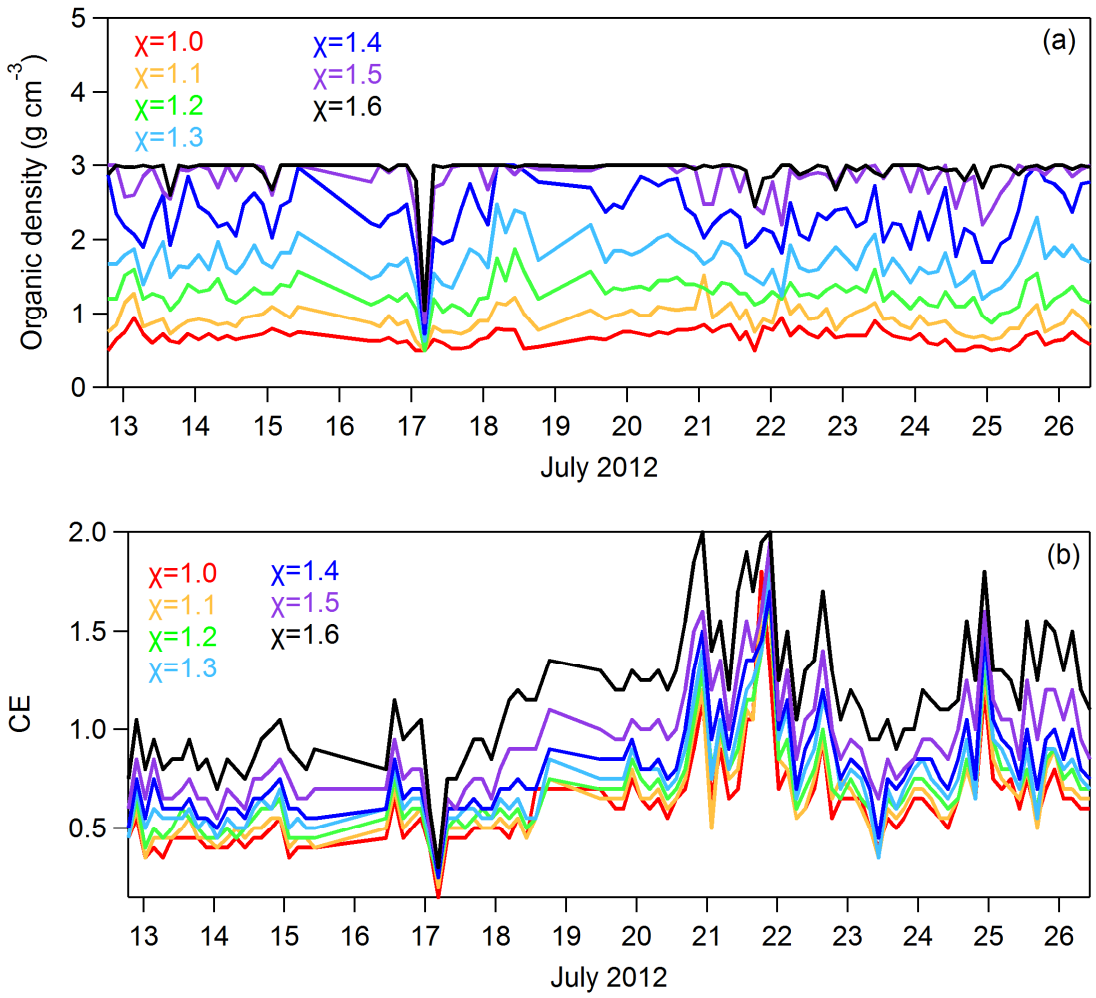

Figure S4. The organic density (a) is quite sensitive to the shape factor, while CE (b) changes for χ greater than 1.3 (Athens).

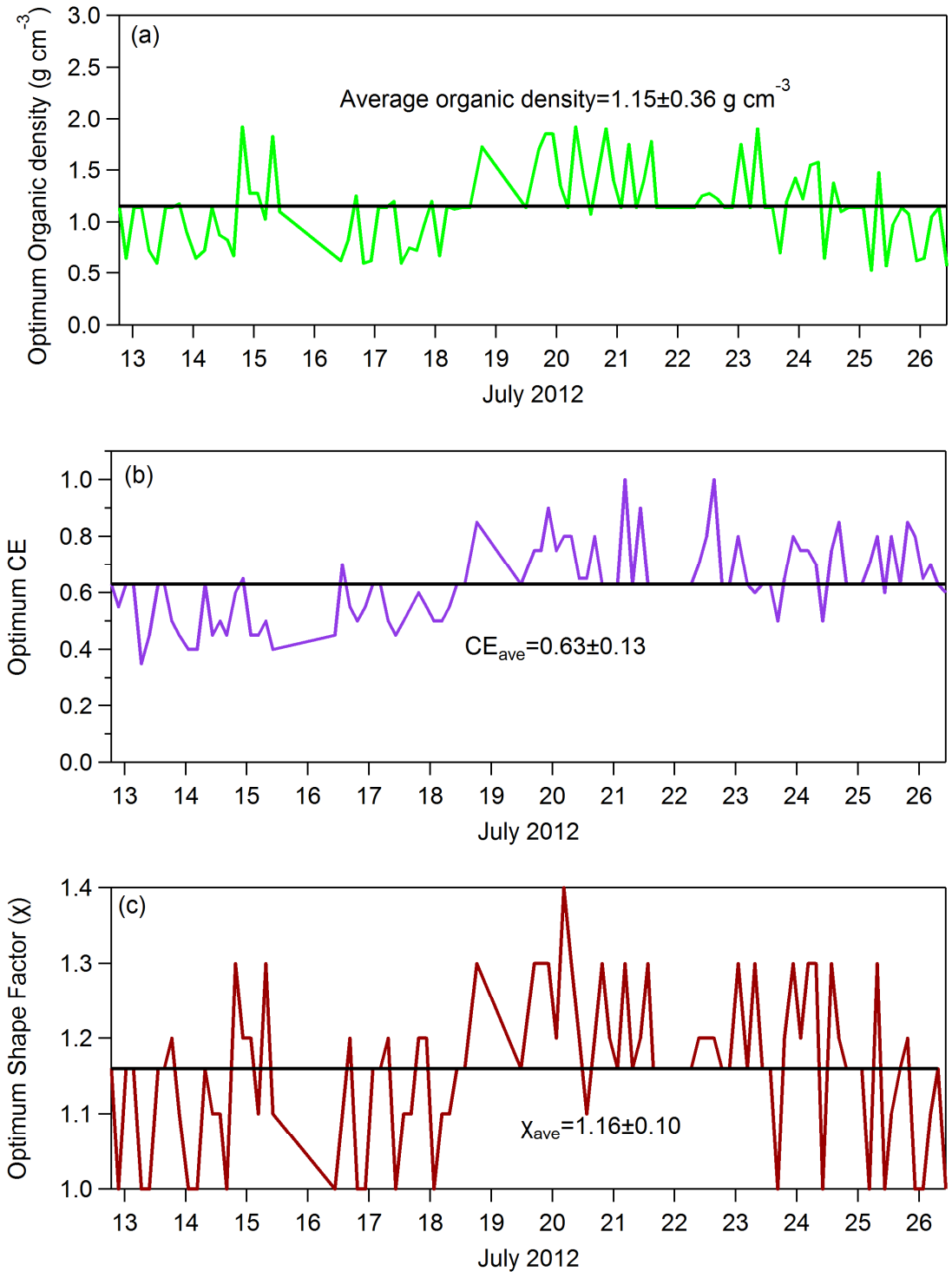

Figure S5. The optimum organic density (a), CE (b) and χ (c) (Athens).

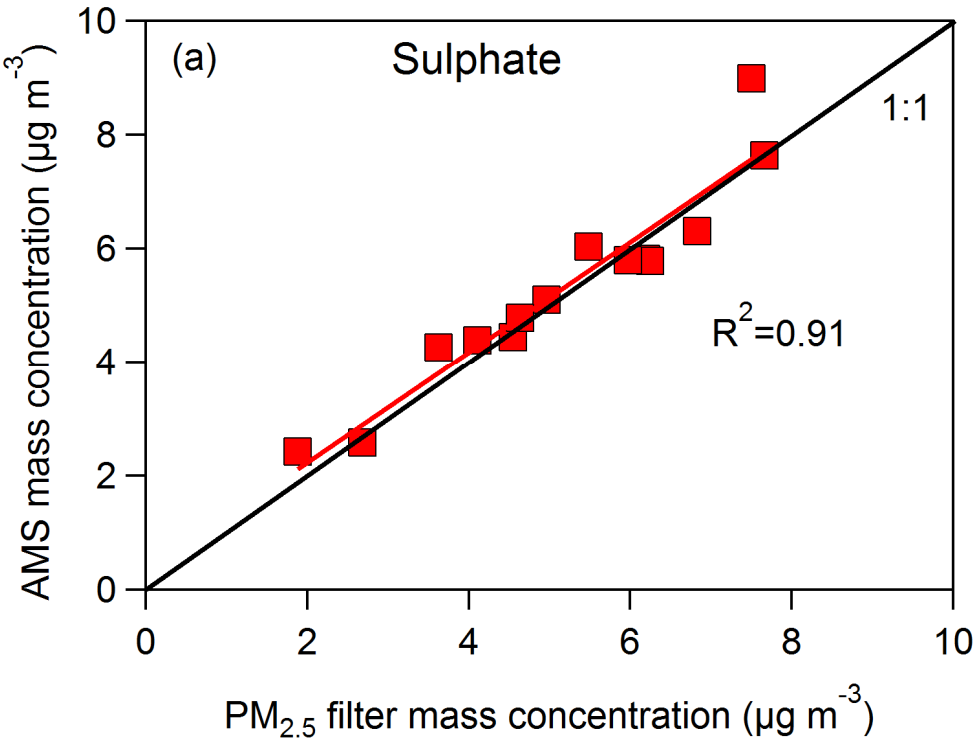

Figure S6. Comparison between the PM_1 AMS sulphate (with CE applied) and the $PM_{2.5}$ filters sulphate for Athens. A high correlation was found (R^2=0.91).

2. Diurnal profiles of OA and BC

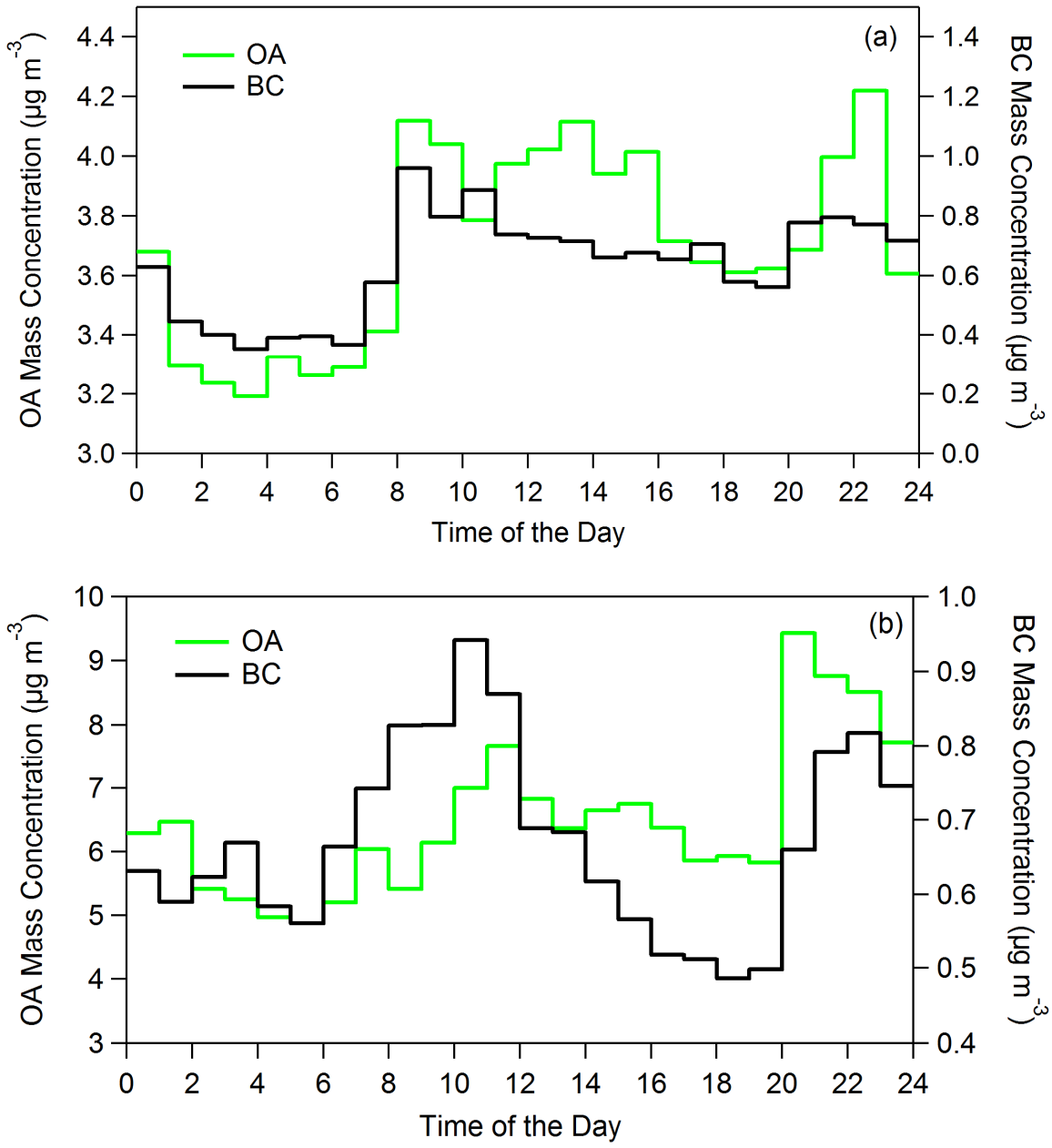

Figure S7. Diurnal profiles of OA and BC a) for Patras and b) for Athens.

3. Fractions of m/z 44 and 57

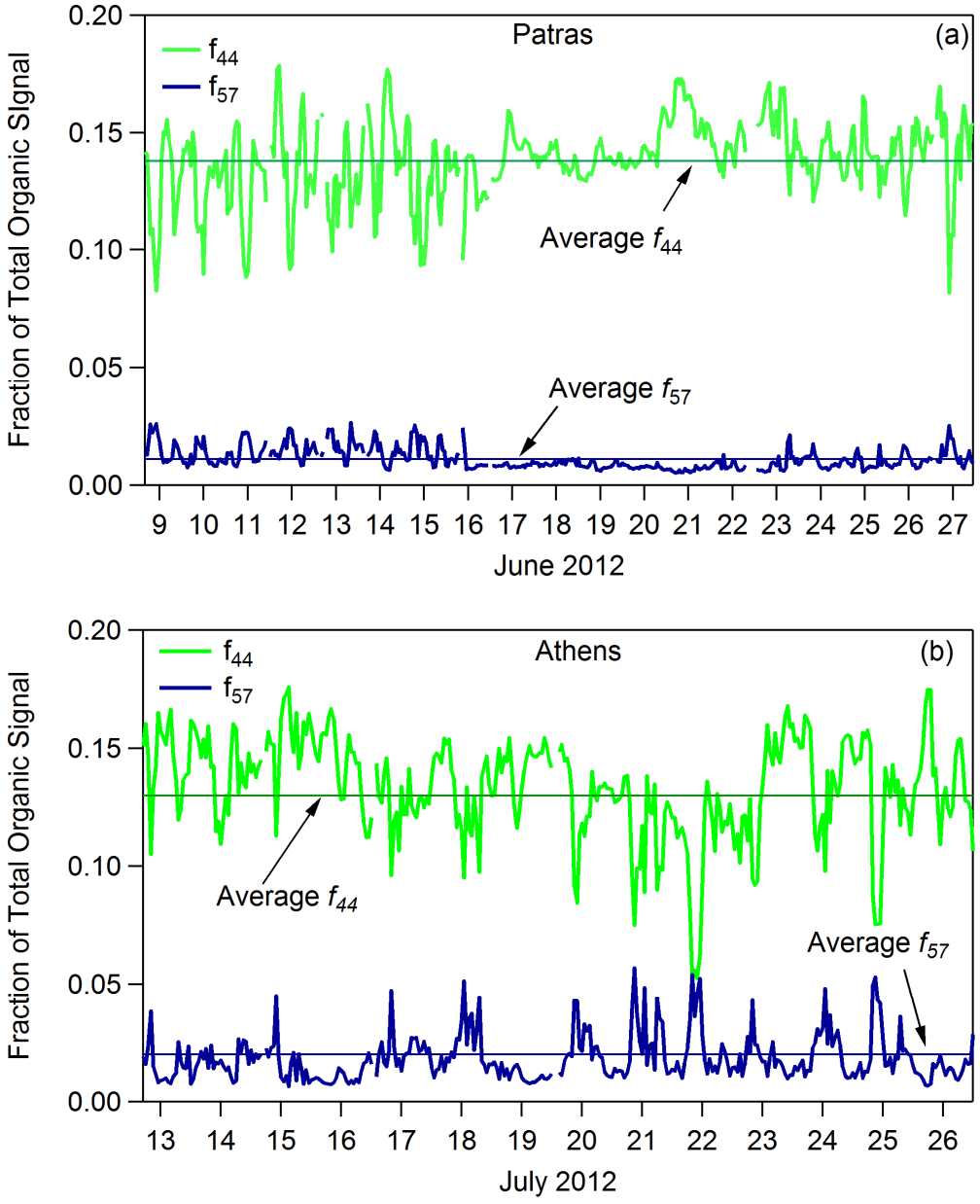

Figure S8. f_{44} and f_{57} time series. a) For Patras the average f_{44} and f_{57} were 0.14 and 0.01 accordingly (a) and in Athens the f_{44} and f_{57} were on average 0.13 and 0.02 correspondingly (b).

4. Organic mass concentration form AMS and filters

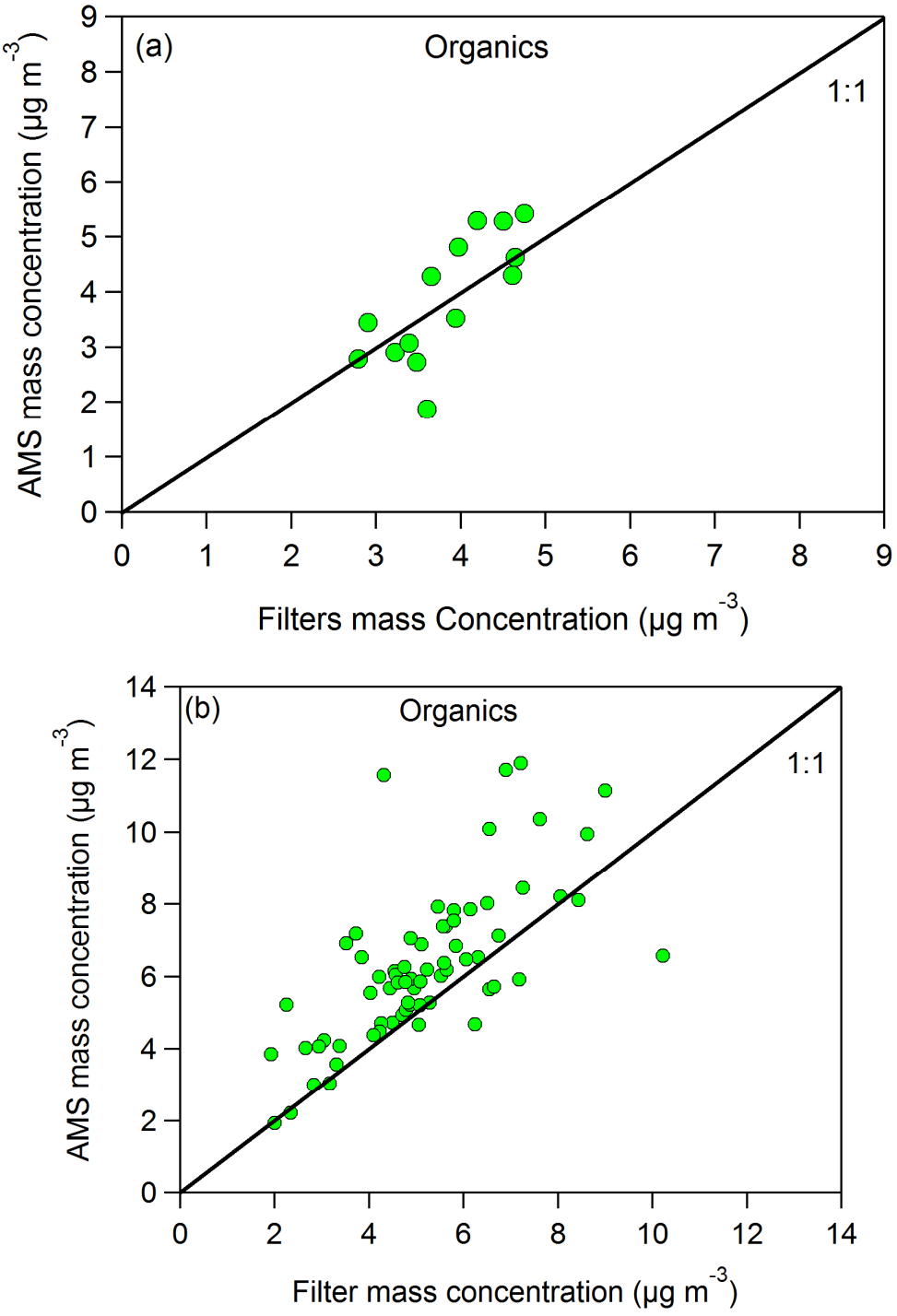

Figure S9. Comparison of the organic mass concentration between the PM_1 AMS (after the CE correction) and the $PM_{2.5}$ filters measurements, after applying the OM:OC ratio from AMS high resolution data a) for Patras and b) for Athens.

5. Estimation of organic nitrate fraction

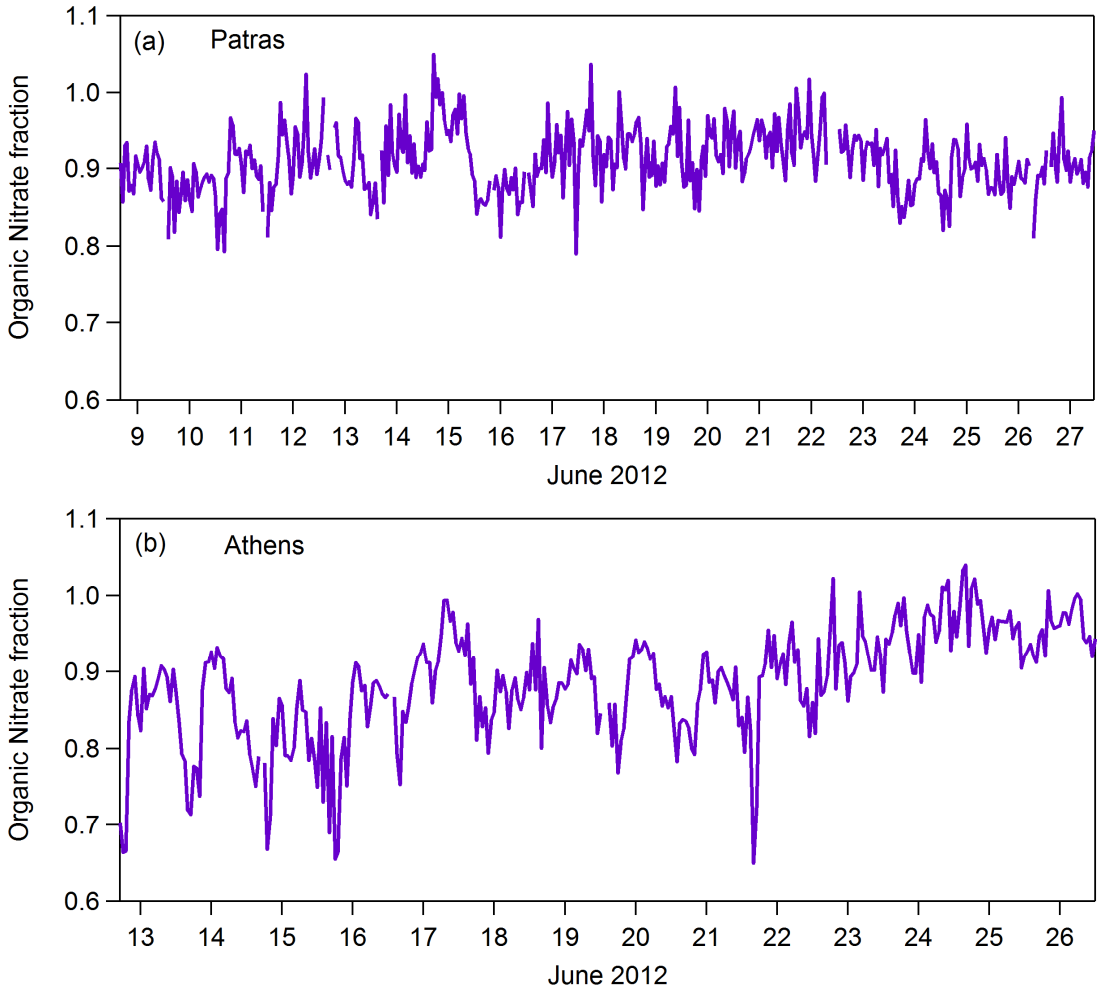

Figure S10. Organic nitrate fraction times series a) in Patras and b) in Athens. In both cities the average organic nitrate fraction was around 90% of the total nitrate.

6. PMF analysis

Both PET (Ulbrich et al., 2009) and ME-2 (Canonaco et al., 2013) tools were used for the PMF factors determination using the HR organic mass spectra. The selection of the solution depended on the characteristics of the mass spectra and on the correlations of the factor time series with specific tracers.

A. Patras

The model residuals using PET for 1 to 5 factors solution are shown in Figures S11 and S12. Moving from 1 to 2 and from 2 to 3 factors the reduction in the residuals is important. The 4 factor residuals are slightly lower especially for 16 and 25 June 2012 in comparison with the 3 factorial residuals, so the 4 factor choice would seem more appropriate, since the 4 and 5 factor residuals do not have notable difference each other. The $Q/Q_{expected}$ versus the number of the factors is illustrated in Figure S13.

For the 4 factor solution the minimum $Q/Q_{expected}$ corresponds to an f_{peak}=0.0 (not shown). In this case 17 out of 20 seeds resulted in the factors: HOA-1, b-OOA, M-OOA and V-OOA (Figure S14a). However, the HOA-1 mass spectrum contained oxygenated species at the *m/z* 43 (22%) and at *m/z* 55 (25%), which is not common for an HOA spectrum (e.g. Sun et al., 2011; Mohr et al., 2012). 3 out of 20 seeds gave the factors: HOA-1, HOA-2, M-OOA and V-OOA (Figure S14b). In this case the f_{44} of the HOA-1 is higher than the f_{43} and the oxygenated part of *m/z* 43 and 55 are 30 and 15% correspondingly. For the reasons above we rejected the 4 factorial solution.

Moving to 5 factors for f_{peak}=0.0 (where $Q/Q_{expected}$ is minimized, Figure S15) the factors extracted are: HOA-1, HOA-2, b-OOA, M-OOA and V-OOA. 12 out of 20 seeds gave again an HOA-1 factor with oxygenate species contribution at *m/z's* 43 and 55 (22 and 10%) (Figure S16a). 8 out of 20 seeds resulted in an HOA-1 less oxygenated compared to the previous cases (13% in *m/z* 43 and 7% at *m/z* 55) (Figure S16b). The OOA (V-OOA, M-OOA and b-OOA) and primary OA (HOA-1 and HOA-2) fractions of the 4 factor solution (76% and 24% correspondingly) do not change significantly compared to those of the 5 factor case (78% and 22% accordingly). Thus we believe that this is a more appropriate solution for Patras.

The solution of the 3 factors (V-OOA, M-OOA and HOA-1) was rejected as 28% of the *m/z* 43 and 27% of the *m/z* 55 of the HOA spectrum was oxygenated (Figure S17a), and due to the residuals reason described above. We also examined the case of 6 factors. In this case the M-OOA is split in 2 parts with similar f_{44} (0.16 in M1-OOA and 0.15 in M2-OOA) (Figure S17b).

For all cases (3, 4 and 5 factors) PET and ME-2 gave practically the same mass spectra and the same time series (with R^2~0.999).

B. Athens

For Athens measurements a 4-factor solution was selected. Figure S19 and S20 illustrates the model residuals for 1 to 5 factors solution obtained by PET. From 1 to 2 and from 2 to 3 factors there is significant difference in the residuals, while between 4 and 5 factors the reduction is very low. The $Q/Q_{expected}$ versus the number of the factors is illustrated in Figure S21a. For the 4-factor solution we selected an f_{peak}=0.0 as the $Q/Q_{expected}$ is minimized (Figure S21b). The factor time series and corresponding mass spectra from PET and ME-2 are almost identical each other (Figure 22).

The 3 factor solution is shown in Figure S23, where the 3 factors are HOA-1, HOA-2 and OOA. Again the time series and the mass spectra of the factors obtained by PET and ME-2 are identical (not shown). We reject the 3 factorial choice due to the residuals characteristics described above and as most of the recent studies refer that during the summer the OOA is usually split in a more oxygenated and a less oxygenated part (e.g. Aiken et al., 2009; Docherty et al., 2011; Sun et al., 2011; Mohr et al., 2012; Crippa et al., 2013).

The 5 factor selection was investigated as well. Performing PMF analysis with ME-2 we obtained 2 slightly different cases: 11 out of the 20 seeds split the M-OOA into 2 parts, which both of them have similar f_{44} contribution (0.14 for M1-OOA and 0.15 for M2-OOA, Figure S24a). Additionally the diurnal profile of M1-OOA is similar to the HOA-2 profile, and this a second reason we reject this combination (Figure S24b). This is the solution that PET indicates as well (for f_{peak}=0.0, where the $Q/Q_{expected}$ was minimized). For 9 out of 20 seeds the OOA is divided into 3 OOA factors V-OOA, M1-OOA and M2-OOA with f_{44}: 0.20, 0.17 and 0.14 correspondingly (Figure S25a). In this

case the M2-OOA profile resembles the HOA-2 profile, which implies that this factor also include part of the HOA-2 (Figure S25b).

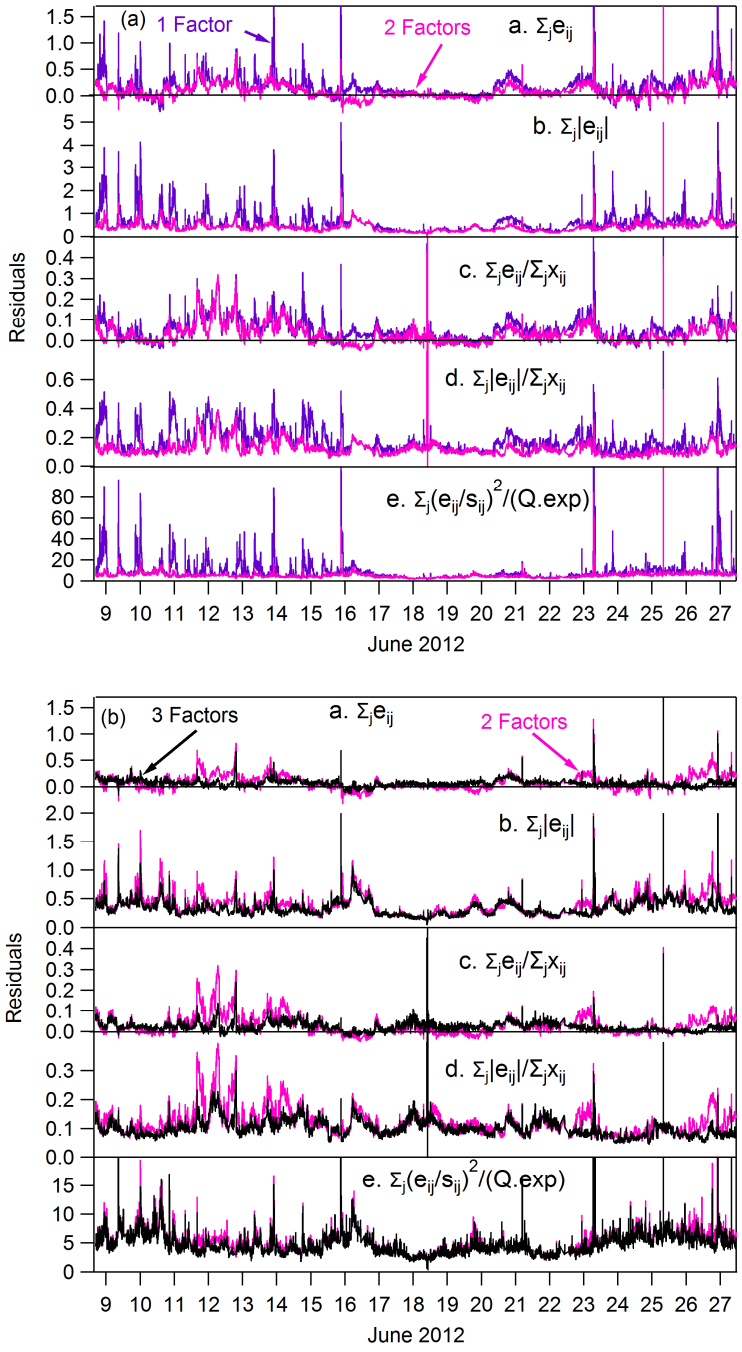

Figure S11. Model residuals **E= X-GF** calculated using the PMF evaluation tool, PET (Ulbrich et al., 2009) for Patras. Comparison between a) 1-factor (purple lines) and 2-factor (pink lines) PMF solution and (b) 2-factor (pink lines) to 3-factor (black lines) PMF solution. The residuals decreased importantly from 1 to 2 factors and from 2 to 3 factors.

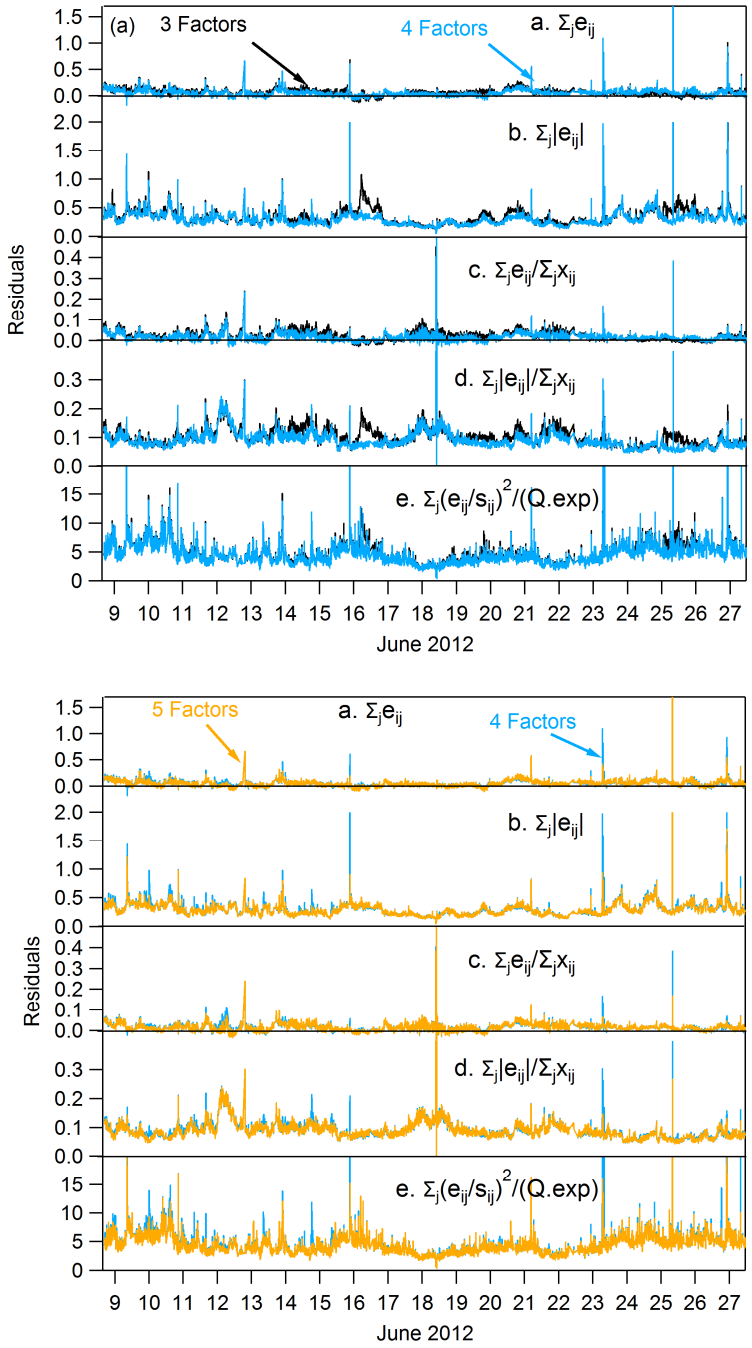

Figure S12. Model residuals **E= X-GF** calculated using the PMF evaluation tool, PET (Ulbrich et al., 2009) for Patras. Comparison between a) 3-factor (black lines) and 4-factor (light blue lines) PMF solutions and (b) 4-factor (light blue lines) and 5-factor (orange lines) PMF solutions. The residuals decreased slightly from 3 to 4 factors for the 16th and 25th June 2012. Between the 4 and 5 factor solution residuals there was only very low change.

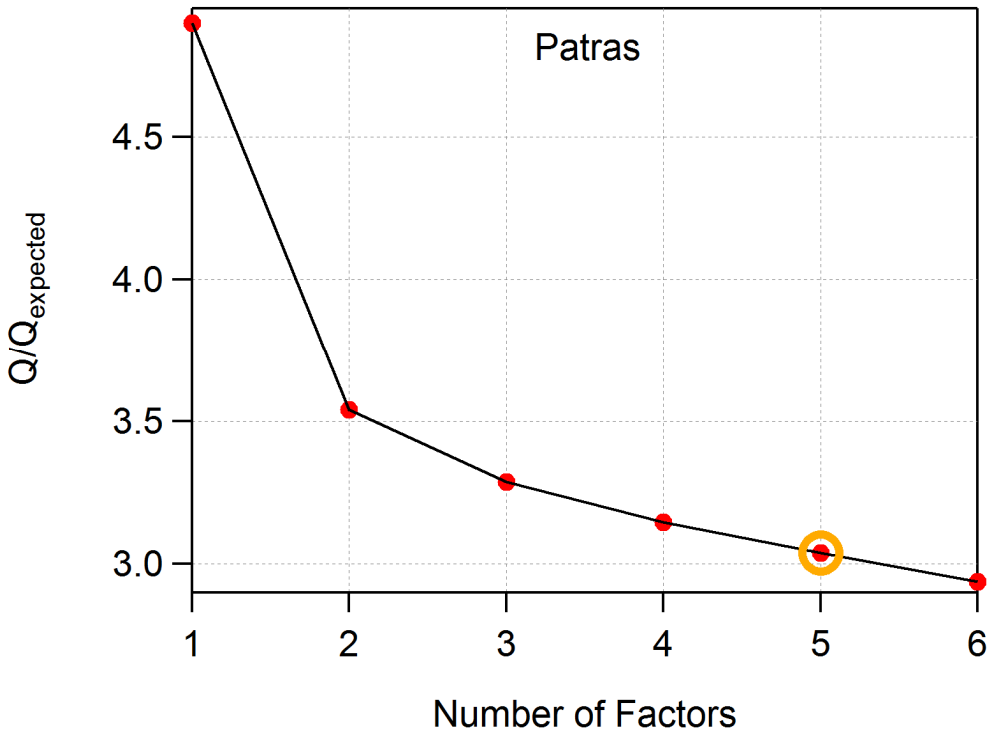

Figure S13. $Q/Q_{expected}$ versus the number of the factors.

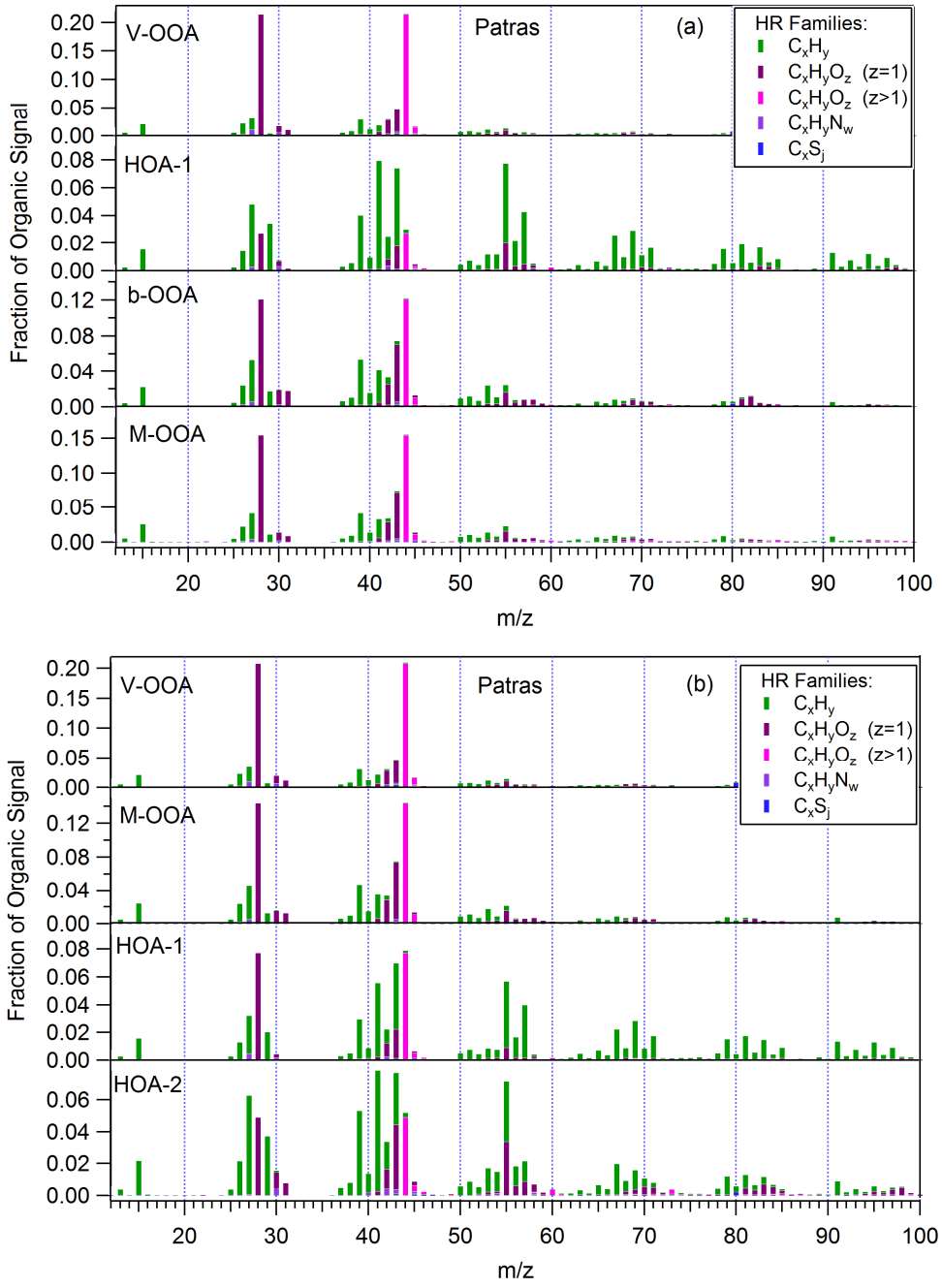

Figure S14. The 4 factor mass spectra a) for the more stable case and b) the less stable case. However, in both combinations the HOA spectrum contains oxygenate species at *m/z's* 43 and 55.

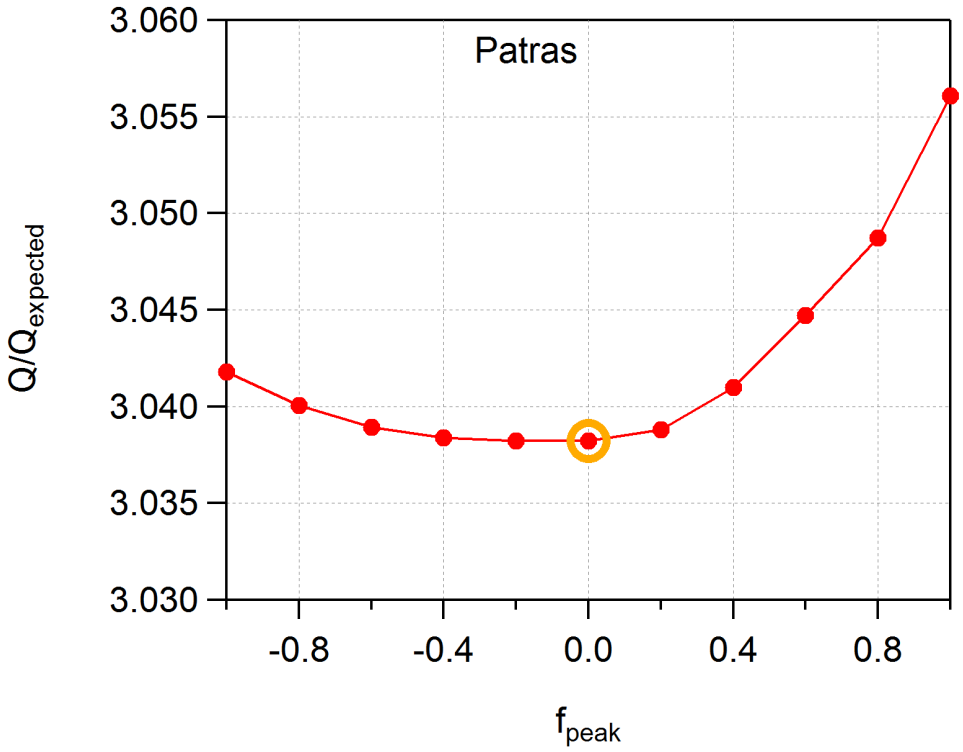

Figure S15. $Q/Q_{expected}$ for f_{peaks} -1 to 1 for a 5 factor solution. There is a stable area between the f_{peaks} -0.4 and 0.0 with lower $Q/Q_{expected}$ at f_{peak}=0.0.

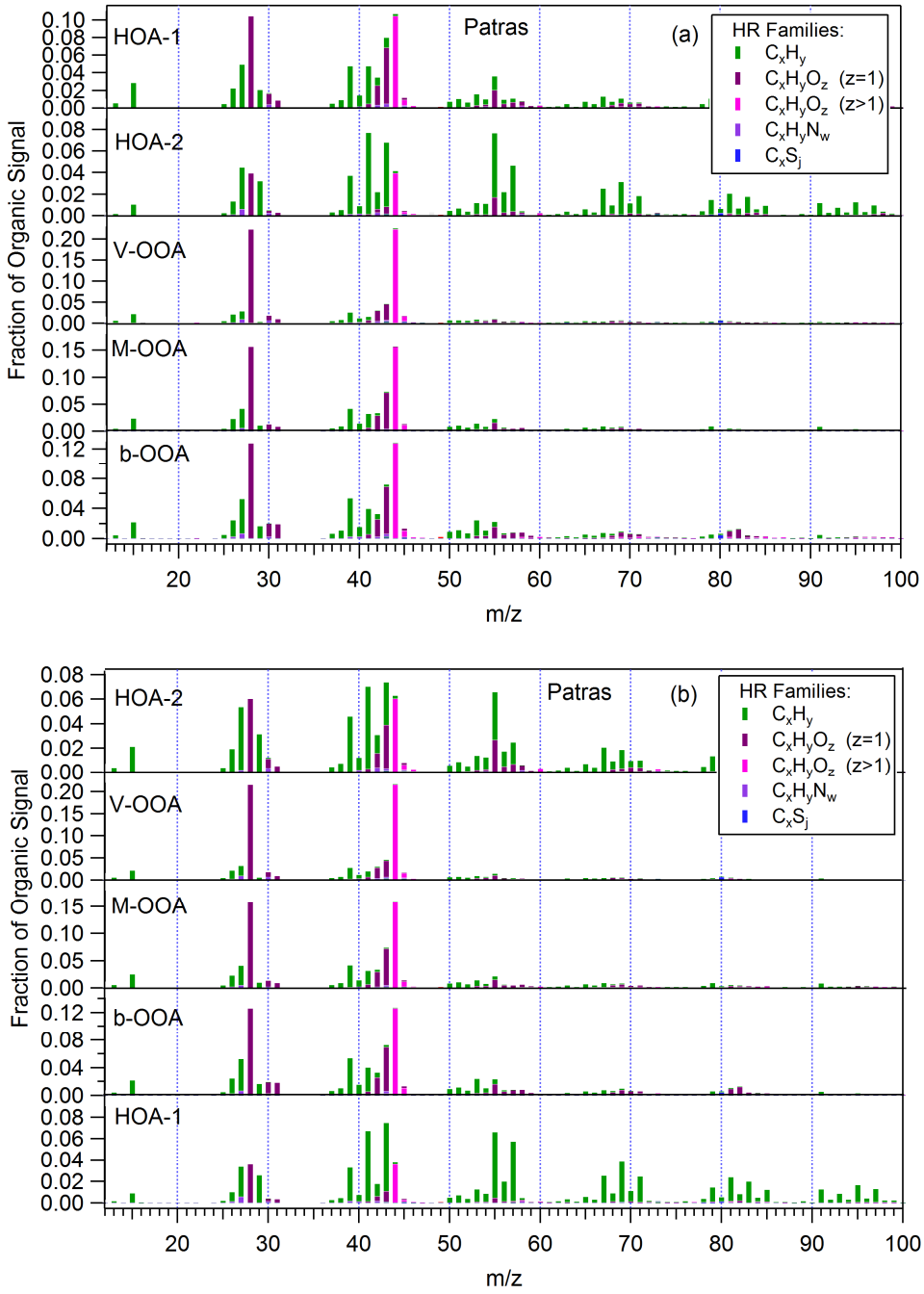

Figure S16. The 5 factor mass spectra for a) 12 out of 20 seeds b) 8 out of 20 seeds. The second option is more appropriate since the HOA-1 mass spectra contains less oxygenated compounds at m/z 43 and 55 compared with the previous case.

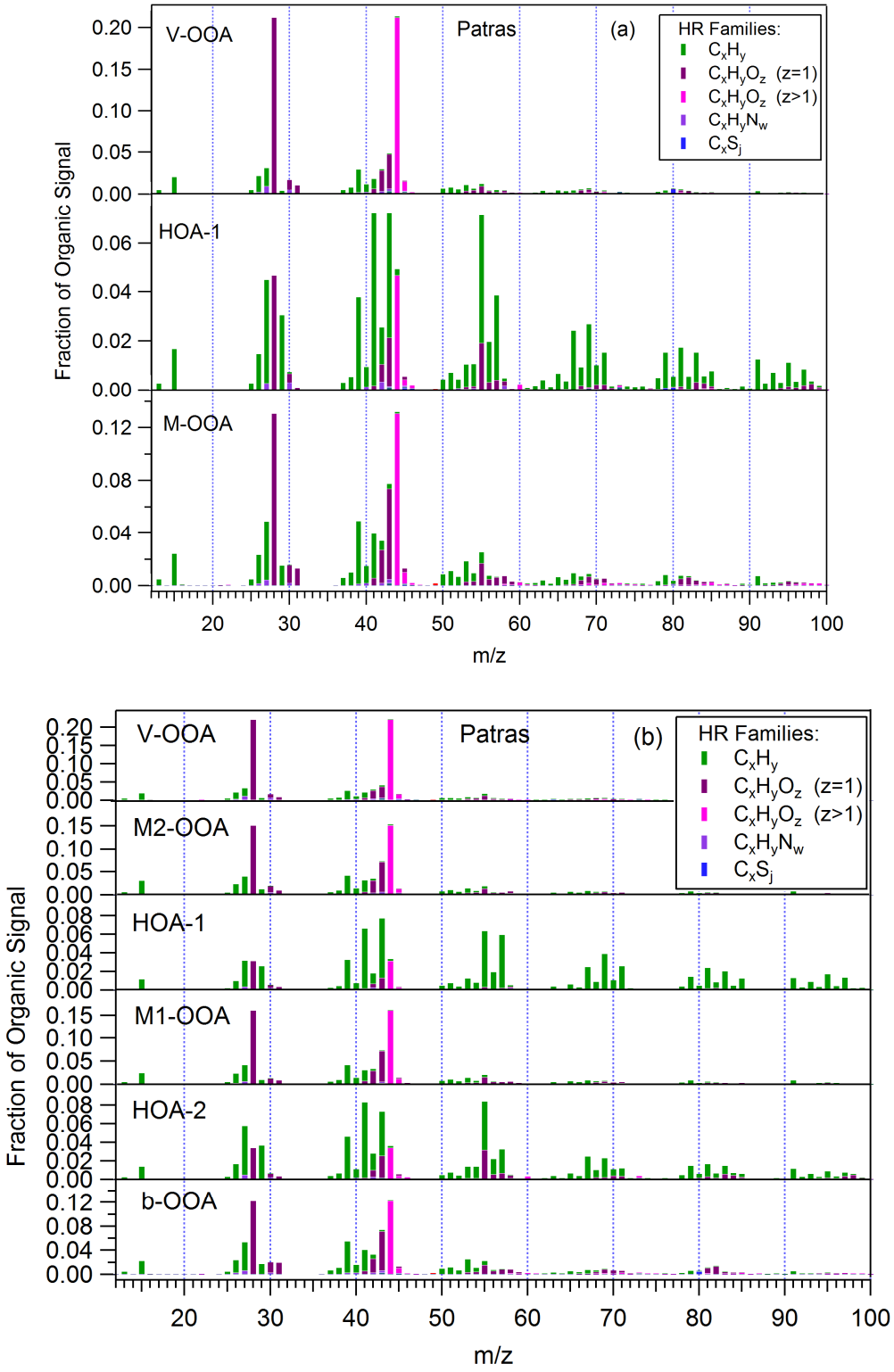

Figure S17. The mass spectra for a) the 3 factor solution which resulted in a oxygenated HOA-1 spectrum and b) the 6 factorial solution, where the M-OOA is split in 2 parts.

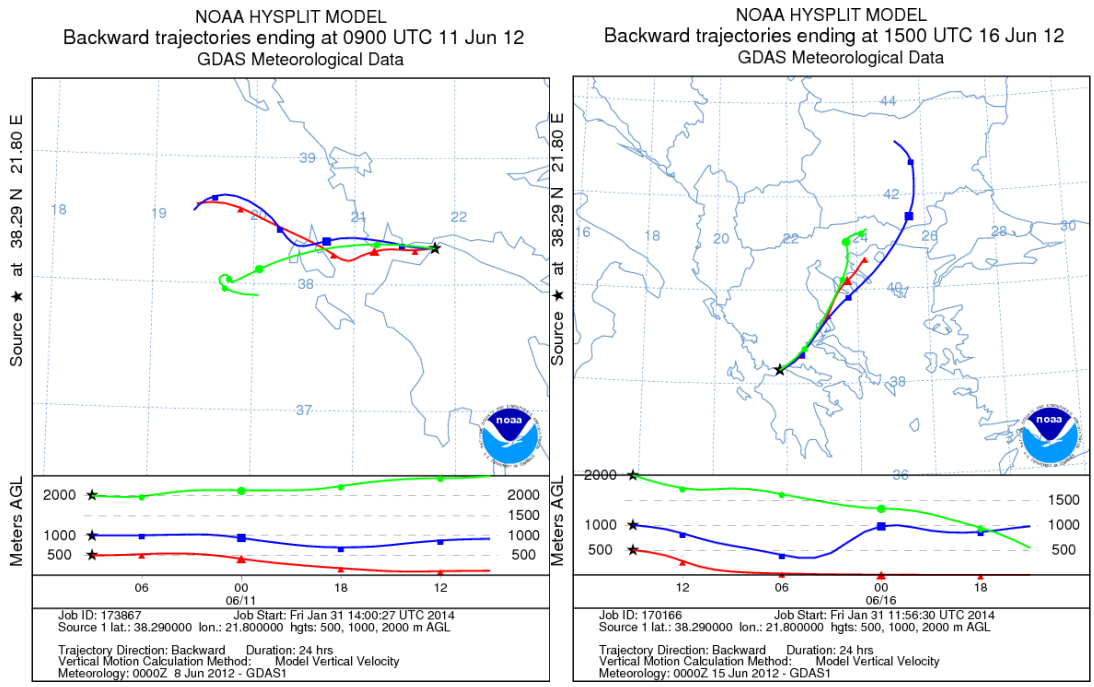

Figure S18. HYSPLIT back trajectories (Draxler and Rolph, 2013). When the air originated from the west (above the Ionian Sea) the b-OOA was minimized, while when the air masses were coming form NE and after have passing though the Central Greece mountains the b-OOA increased.

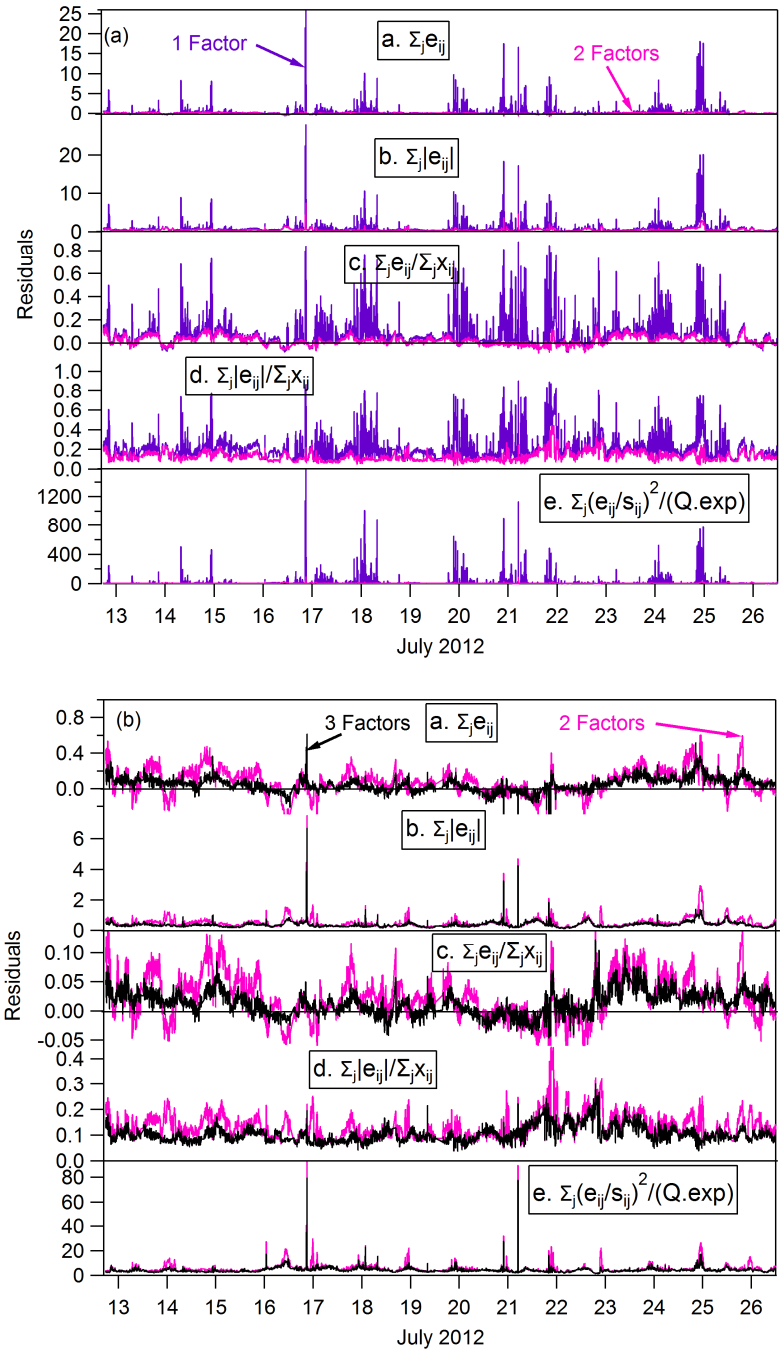

Figure S19. Model residuals **E= X-GF** calculated using the PMF evaluation tool, PET (Ulbrich et al., 2009) for Athens. Comparison between a) 1-factor (purple lines) and 2-factor (pink lines) PMF solution and (b) 2-factor (pink lines) to 3-factor (black lines) PMF solution. From 1 to 2 factors and from 2 to 3 factors the residuals decreased significantly.

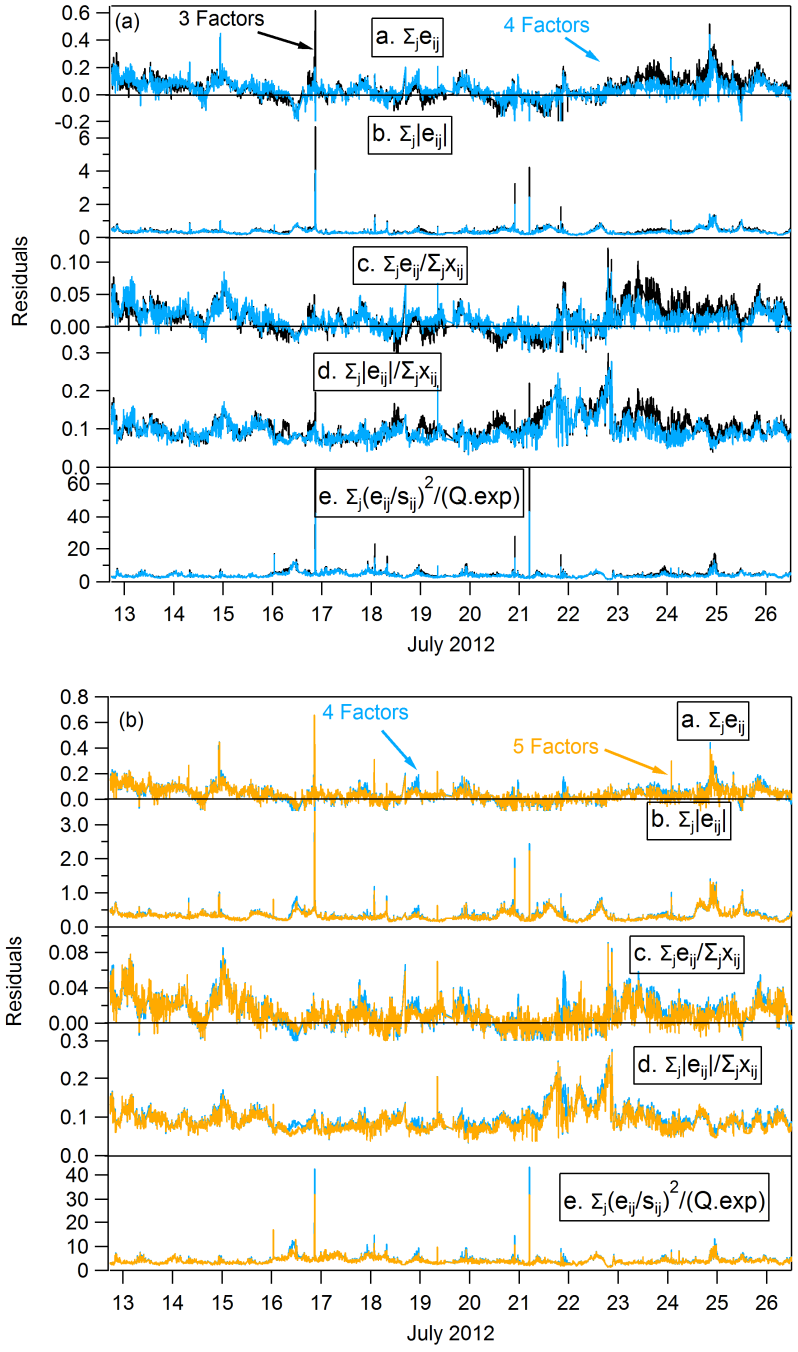

Figure S20. Model residuals **E= X-GF** calculated using the PMF evaluation tool, PET (Ulbrich et al., 2009) for Athens. Comparison between a) 3-factor (black lines) and 4-factor (light blue lines) PMF solutions and (b) 4-factor (light blue lines) and 5-factor (orange lines) PMF solutions. The 4 factor residuals are slightly lower in comparison with the residuals of the 3 factorial solution. The 4 and 5 factor solution residuals had very low difference.

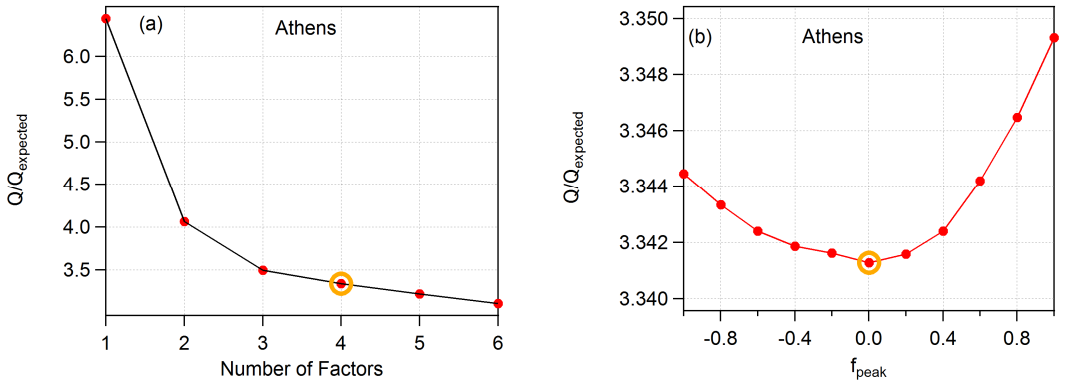

Figure S21. $Q/Q_{expected}$ versus the number of the factors (a) $Q/Q_{expected}$ for f_{peaks} -1 to 1 for a 4 factor solution (b).

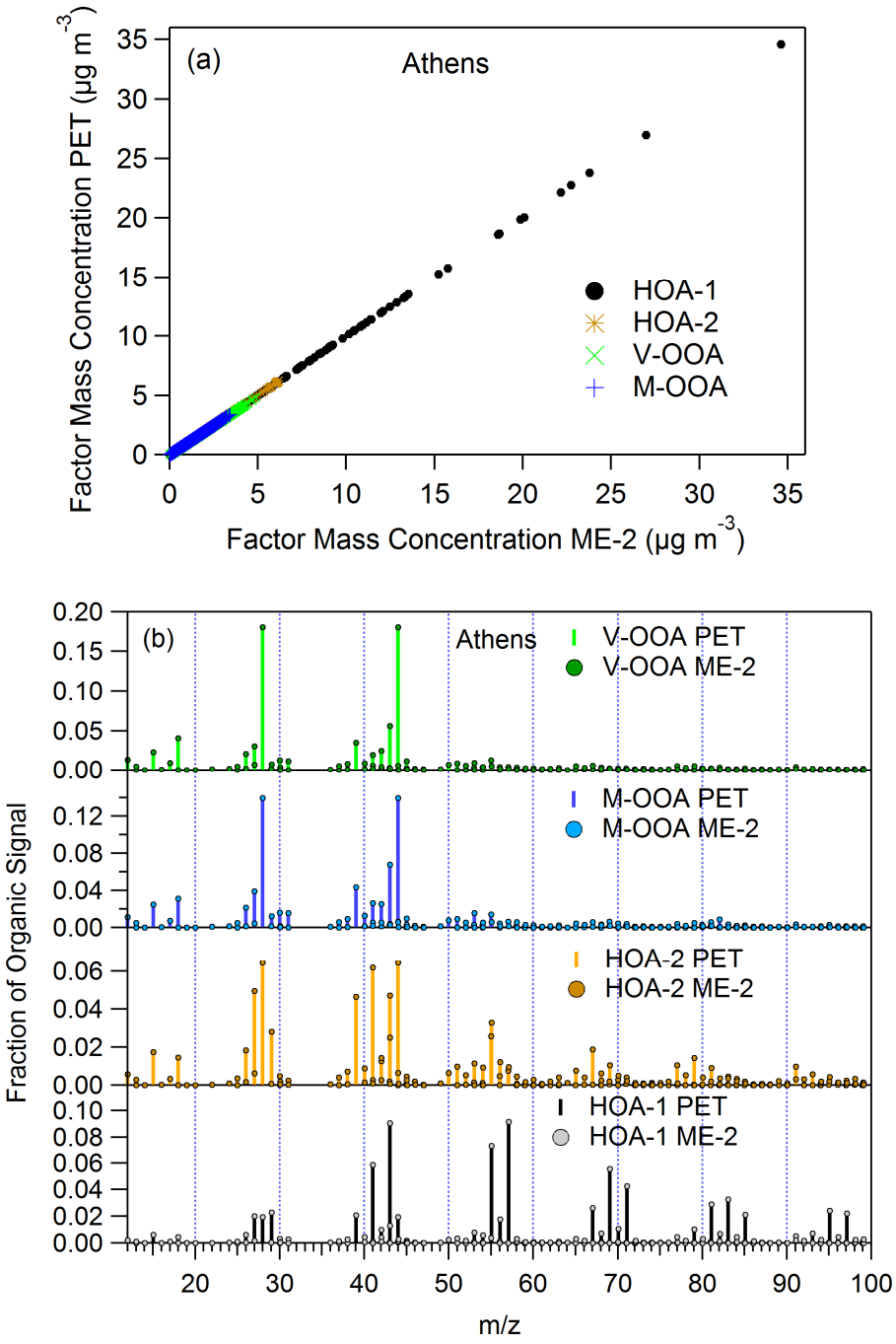

Figure S22. The time series (a) and the mass spectra (b) of the 4 factors calculated by PET are almost identical to the 4 factors obtained by ME-2.

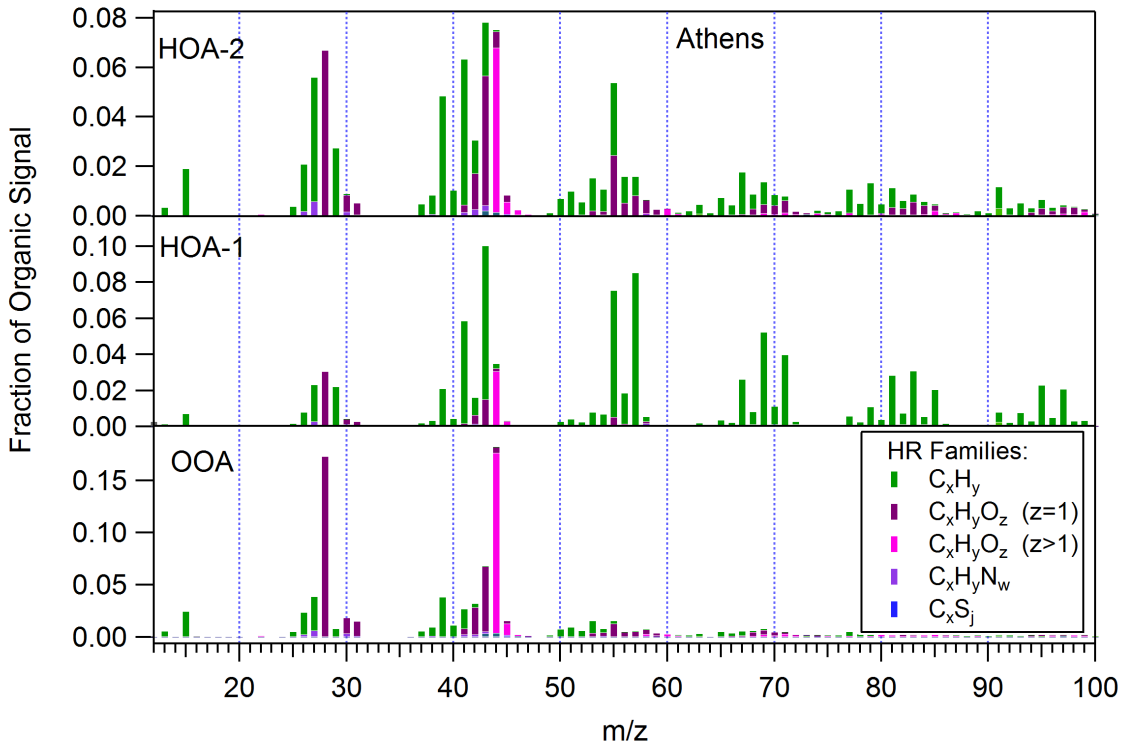

Figure S23. The 3 factor PMF solution for f_{peak}=0.0.

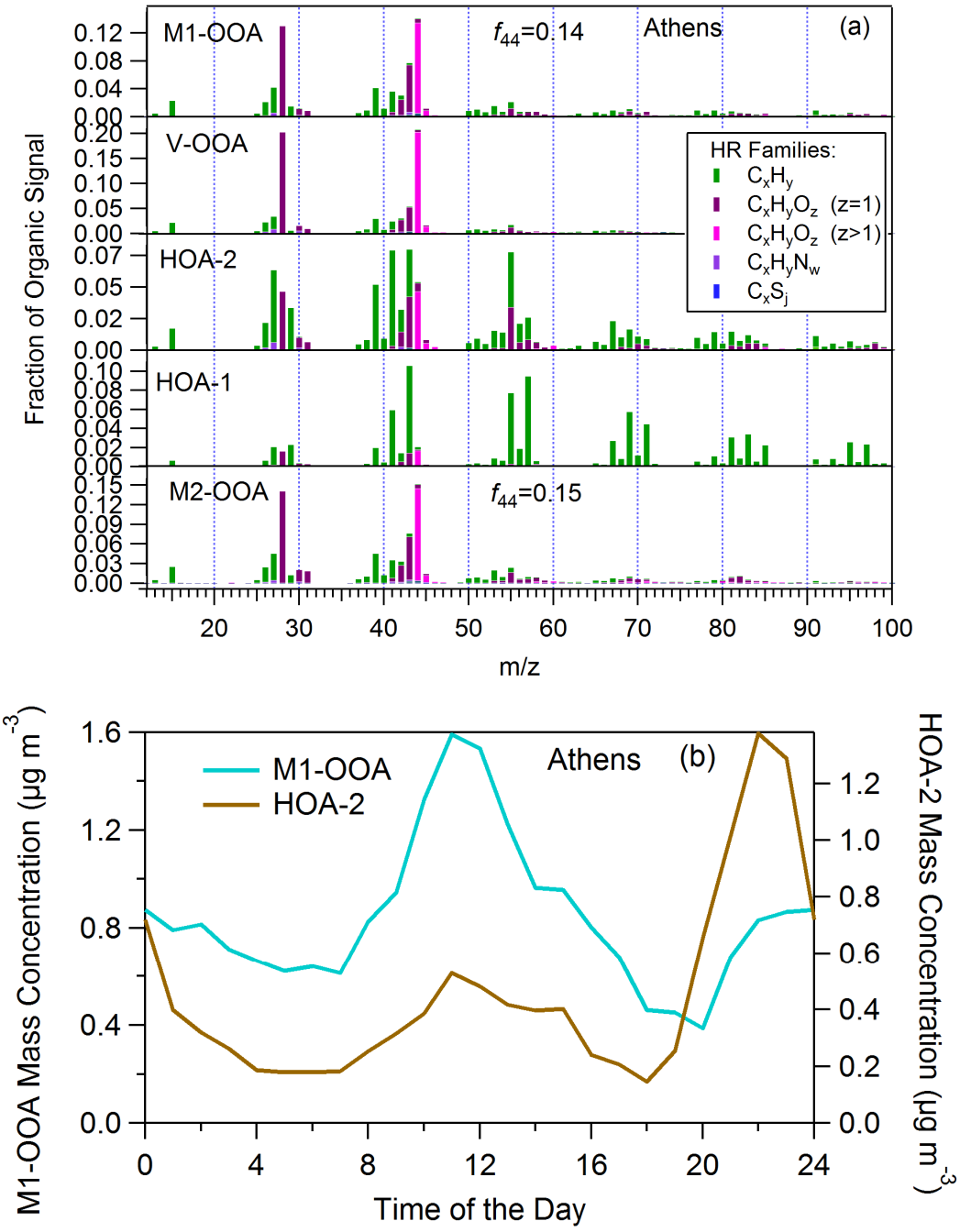

Figure S24. (a) The 5 factor PMF solution for 11 out of 20 seeds. The M-OOA into 2 parts, which both of them have similar f_{44} contribution (0.14 for M1-OOA and 0.15 for M2-OOA. (b) The diurnal profile of M1-OOA is similar to the HOA-2 profile.

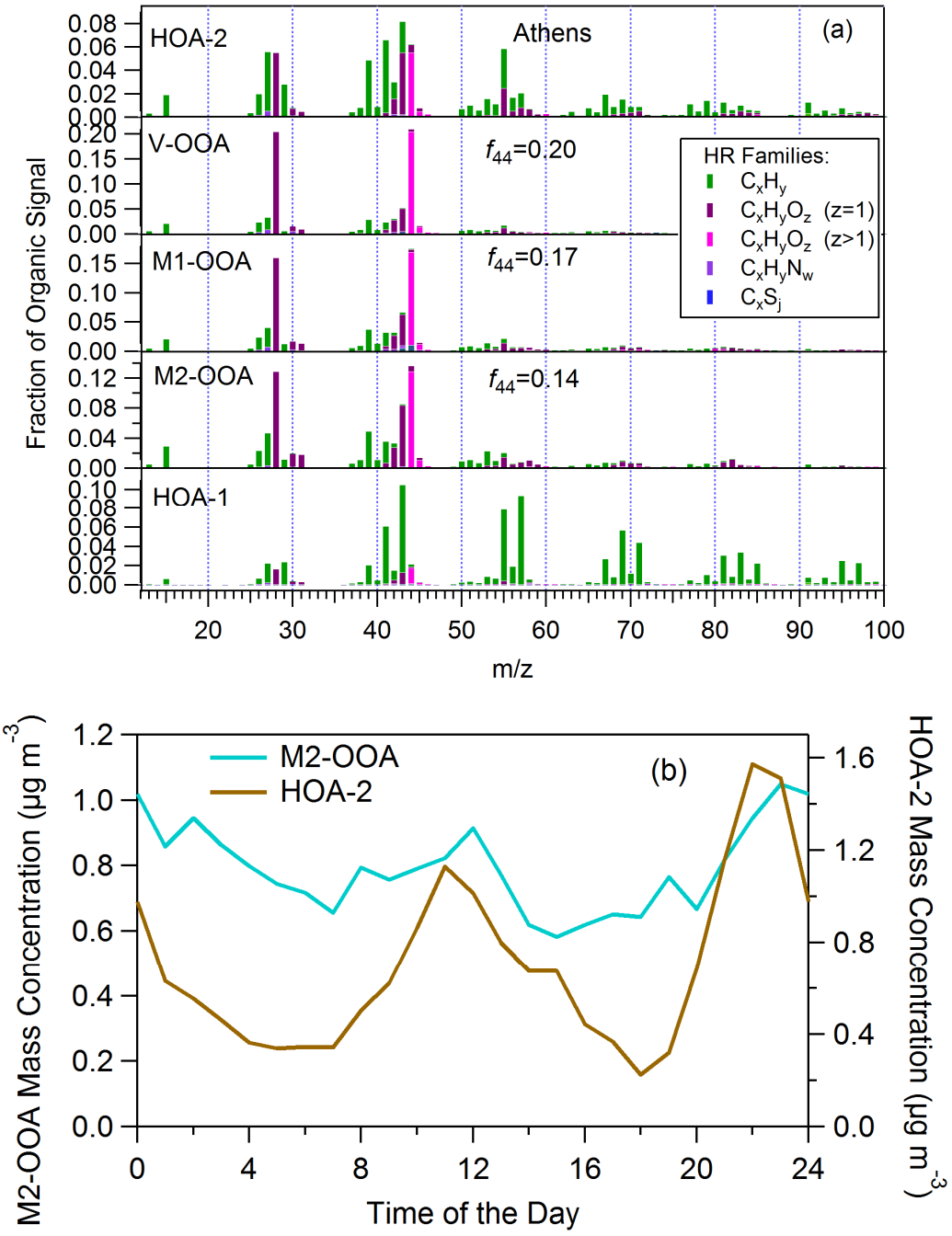

Figure S25. (a) The 5 factor PMF solution for 9 out of 20 seeds. The OOA is divided into 3 parts with f_{44}: 0.20, 0.17 and 0.14 correspondingly. (b) The M2-OOA profile resembles the HOA-2 profile.

7. Rose plots for Athens

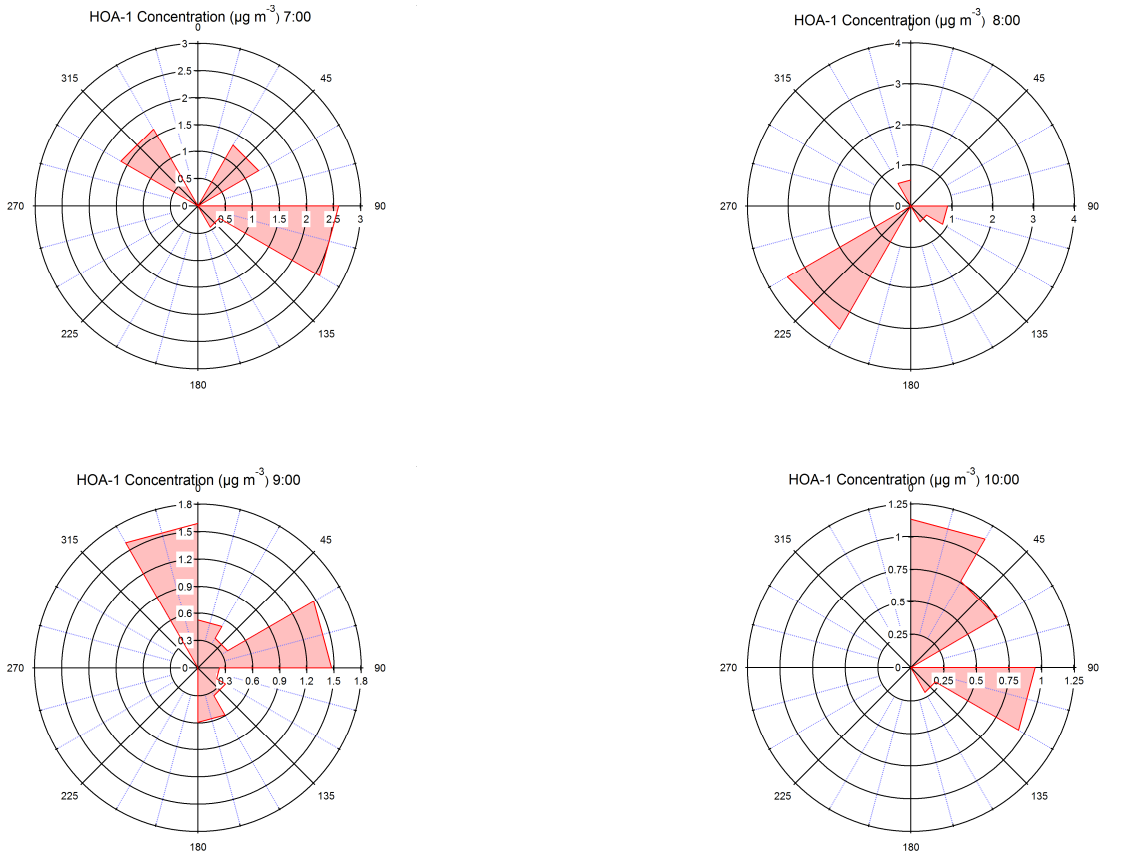

Figure S26. Rose plots for HOA for 7:00-10:00 for wind speeds greater than 1 m s^{-1}.

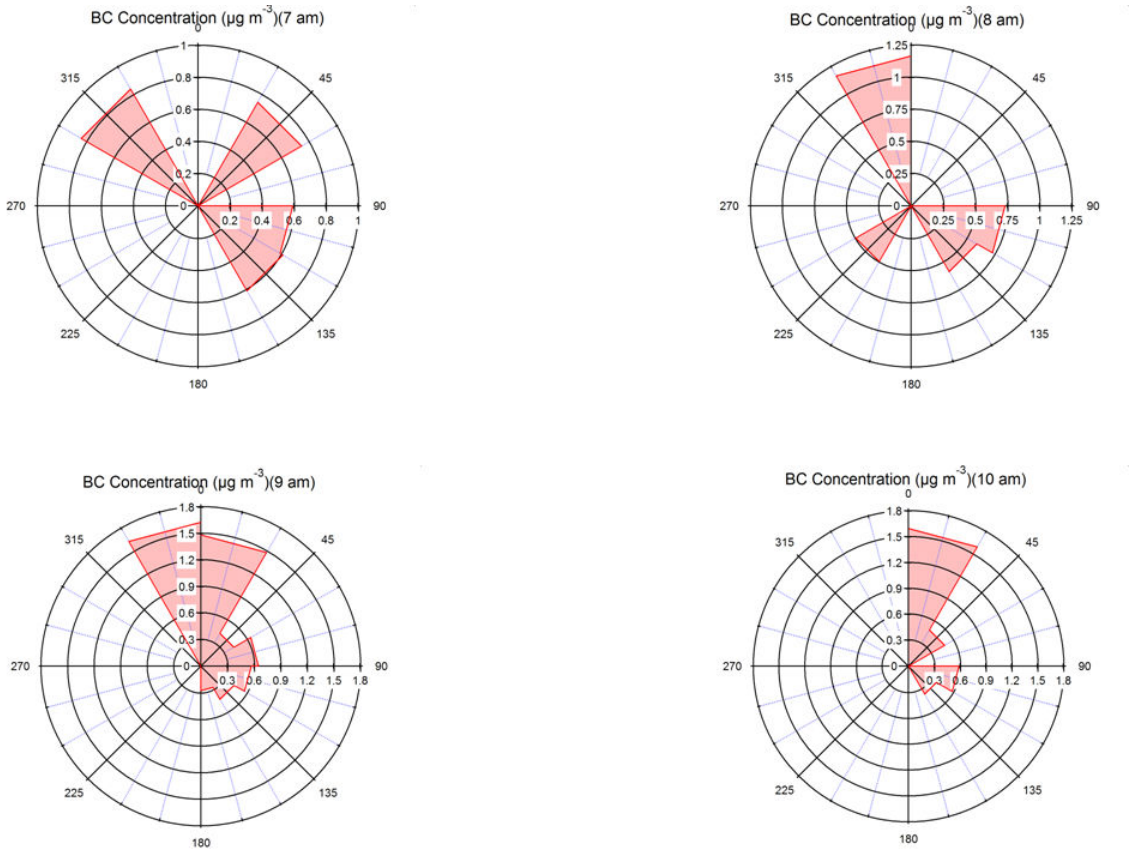

Figure S27. Rose plots for BC for 7:00-10:00 for wind speeds greater than 1 m s^{-1}.

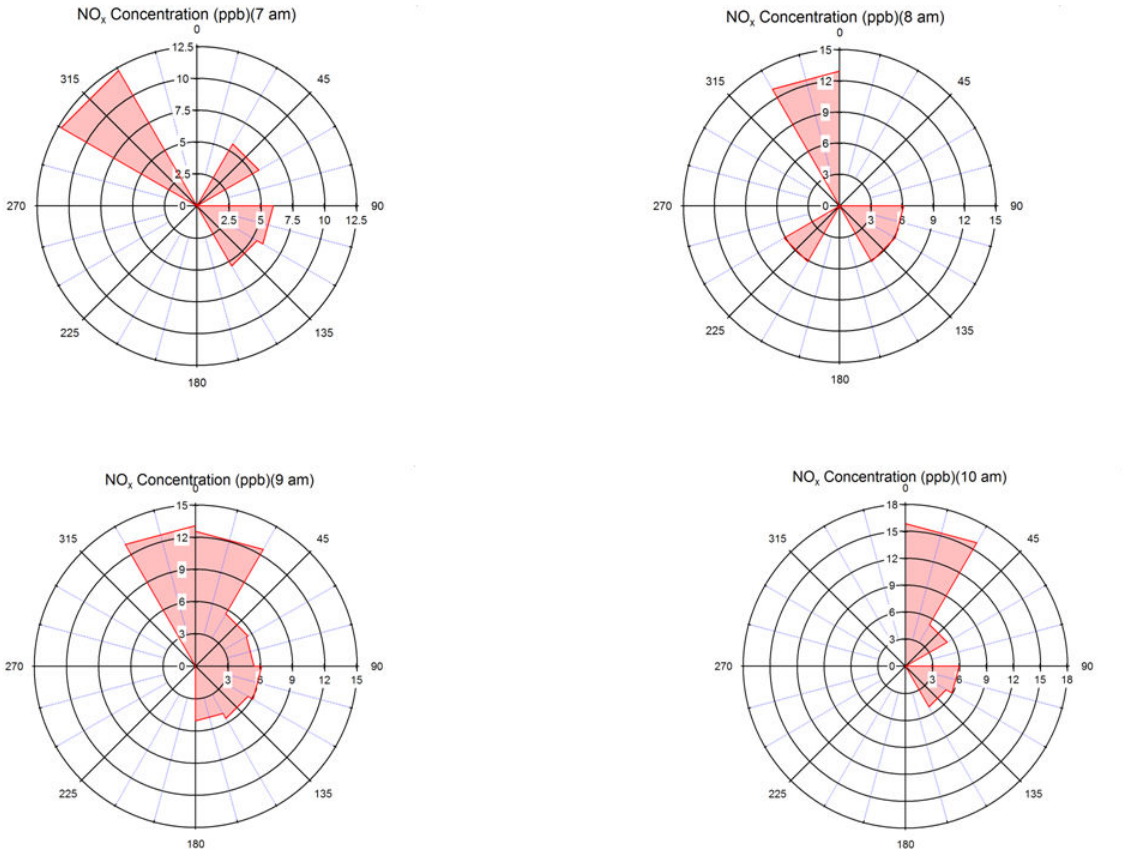

Figure S28. Rose plots for NO_x for 7:00-10:00 for wind speeds greater than 1 m s^{-1}.

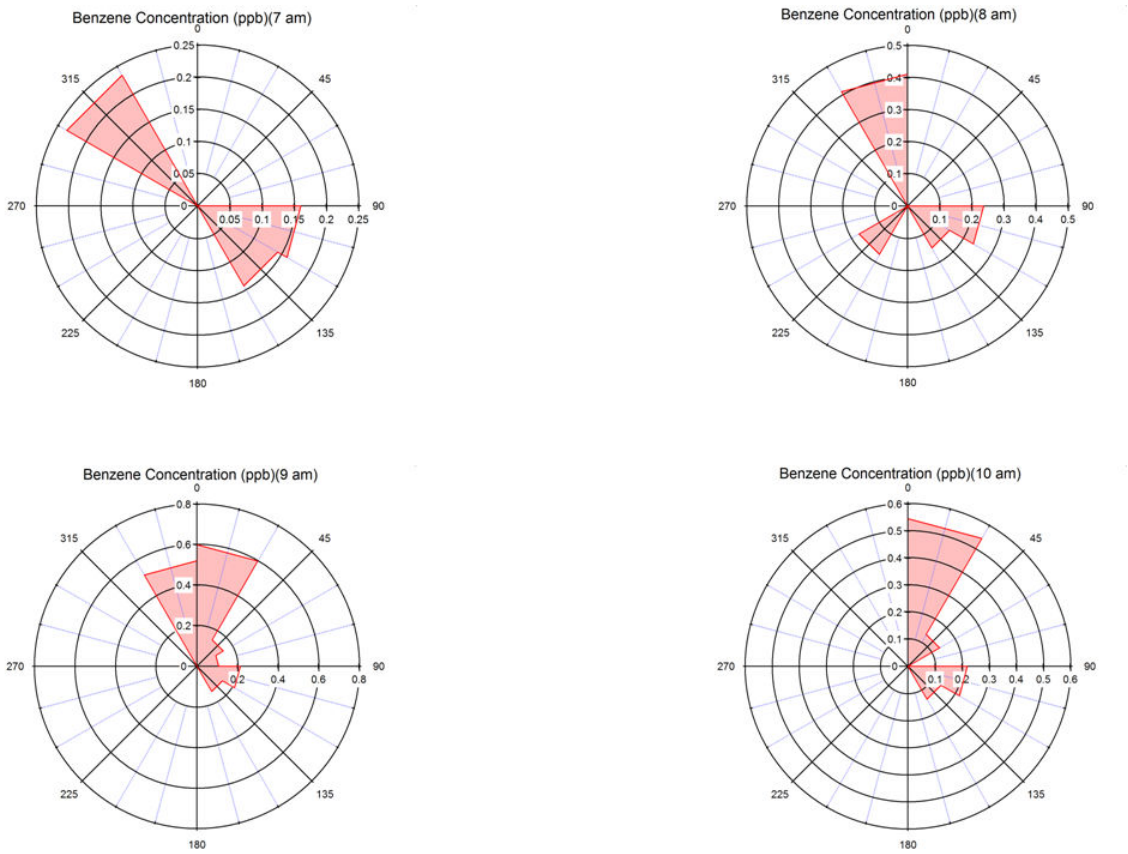

Figure S29. Rose plots for benzene for 7:00-10:00 for wind speeds greater than 1 m s^{-1}.

8. FLEXPART analysis

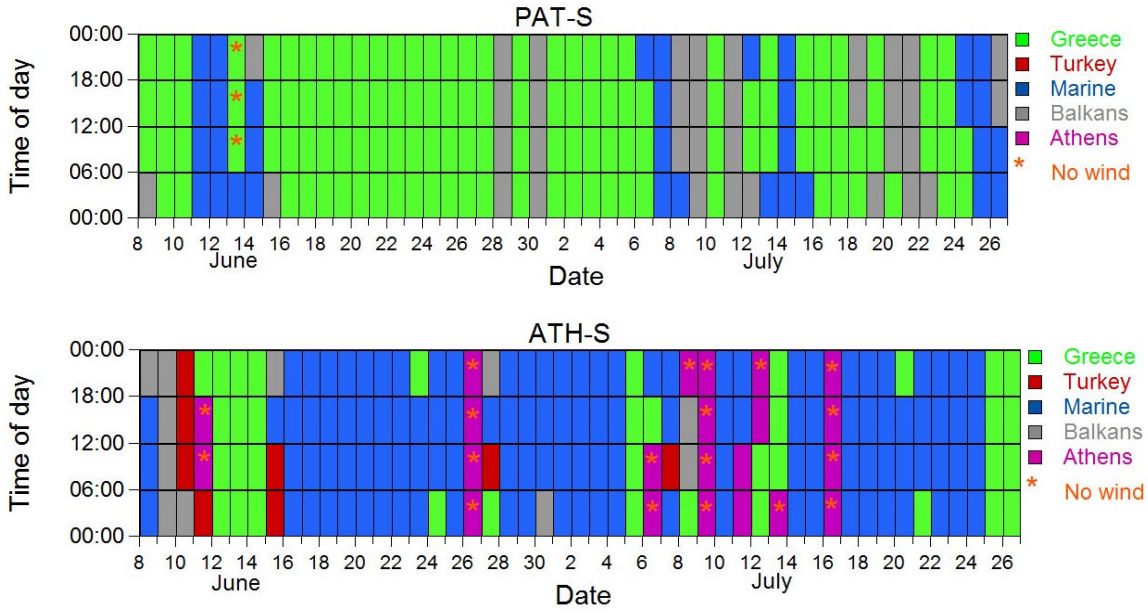

Figure S30: FLEXPART analysis (Stohl et al., 2005) for Patras and Athens campaigns.

References

Aiken, A. C., Salcedo, D., Cubison, M. J., Huffman, J. A., DeCarlo, P. F., Ulbrich, I. M., Docherty, K. S., Sueper, D., Kimmel, J. R., Worsnop, D. R., Trimborn, A., Northway, M., Stone, E. A., Schauer, J. J., Volkamer, R. M., Fortner, E., de Foy, B., Wang, J., Laskin, A., Shutthanandan, V., Zheng, J., Zhang, R., Gaffney, J., Marley, N. A., Paredes-Miranda, G., Arnott, W. P., Molina, L. T., Sosa, G., and Jimenez, J. L.: Mexico City aerosol analysis during MILAGRO using high resolution aerosol mass spectrometry at the urban supersite (T0) – Part 1: Fine particle composition and organic source apportionment, Atmos. Chem. Phys., 9, 6633-6653, 2009.

Canonaco, F., Crippa, M., Slowik, J. G., Baltensperger, U., and Prévôt, A. S. H.: SoFi, an IGOR-based interface for the efficient use of the generalized multilinear engine (ME-2) for the source apportionment: ME-2 application to aerosol mass spectrometer data, Atmos. Meas. Tech., 6, 3649-3661, 2013.

Crippa M., El Haddad I., Slowik J., G., DeCarlo P. F., Mohr, C., Heringa, M., F, Chirico, R., Marchand, N., Sciare, J., Urs, B., and Prévôt, A. S. H.: Identification of marine and continental aerosol sources in Paris using high resolution aerosol mass spectrometry, J. Geophys. Res, doi: 118, 1950-1963, doi: 10.1002/jgrd.50151, 2013.

Docherty, K. S., Aiken, A. C., Huffman, J. A., Ulbrich, I. M., DeCarlo, P. F., Sueper, D., Worsnop, D. R., Snyder, D. C., Peltier, R. E., Weber, R. J., Grover, B. D., Eatough, D. J., Williams, B. J., Goldstein, A. H., Ziemann, P. J., and Jimenez, J. L.: The 2005 Study of Organic Aerosols at Riverside (SOAR-1): Instrumental intercomparisons and fine particle composition, Atmos. Chem. Phys., 11, 12387-12420, 2011.

Draxler, R. R., and Rolph, G. D., 2013. HYSPLIT (HYbrid Single-Particle Lagrangian Integrated Trajectory) Model access via NOAA ARL READY Website (http://ready.arl.noaa.gov/HYSPLIT.php). NOAA Air Resources Laboratory, Silver Spring, MD.

Kostenidou, E., Pathak, R. K., and Pandis, S. N.: An algorithm for the calculation of secondary organic aerosol density combining AMS and SMPS data, Aerosol Sci. Technol., 41, 1002–1010, 2007.

Mohr, C., DeCarlo, P. F., Heringa, M. F., Chirico, R., Slowik, J. G., Richter, R., Reche, C., Alastuey, A., Querol, X., Seco, R., Penuelas, J., Jimenez, J. L., Crippa, M., Zimmermann, R., Baltensperger, U., and Prevot, A. S. H.: Identification and quantification of organic aerosol fromcooking and other sources in Barcelona using aerosol mass spectrometer data, Atmos. Chem. Phys., 12, 1649–1665, 2012.

Stohl, A., Forster, V., Frank, A., Seibert, P., & Wotawa, G.: Technical Note: The Lagrangian particle dispersion model FLEXPART version 6.2, Atmos. Chem. Phys., 5, 2461–2474, 2005.

Sun, Y. L., Zhang, Q., Schwab, J. J., Demerjian, K. L., Chen, W. N., Bae, M. S., Hung, H. M., Hogrefe, O., Frank, B., Rattigan, O. V., and Lin, Y. C.: Characterization of the sources and processes of organic and inorganic aerosols in New York city with a high-resolution time-of-flight aerosol mass spectrometer, Atmos. Chem. Phys., 11, 1581–1602, 2011.

Ulbrich, I. M., Canagaratna, M. R., Zhang, Q., Worsnop, D. R., and Jimenez, J. L.: Interpretation of organic components from Positive Matrix Factorization of aerosol mass spectrometric data, Atmos. Chem. Phys., 9, 2891–2918, 2009.